

APS

Single-Loop Multi-Dimensional Digital Feedback by FIR Filters

T. Nakamura

*Japan Synchrotron Radiation Research Institute/SPring-8,
1-1-1 Kouto, Sayo-cho, Sayo-gun, Hyogo 679-5198, Japan*

(Dated: February 26, 2009)

Abstract

We propose single-loop multi-dimensional feedback with digital signal processing using finite impulse response (FIR) filters. With this scheme, a feedback controls beam oscillations multi-dimensionally with a single beam position signal and a single kick signal. This scheme simplifies the feedback system and reduces the number of components, related tuning points, and cost. Single-loop horizontal and vertical two-dimensional transverse feedback systems based on this scheme are in operation at several storage rings. We also show a scheme of a longitudinal feedback with a transverse feedback system which measures the position at a dispersive section to detect energy shift and kicks transversely at a dispersive section to change the circumference of a ring. This leads to an idea of a single-loop three-dimensional feedback including longitudinal motion and we discussed the possibility of this scheme by showing the ratio of the transverse and longitudinal dynamic range and required power. For the calculation of the coefficients of FIR filters for such feedback systems, we developed a time domain least square fitting method and, with this method, we can make FIR filters with arbitrary large number of taps with which we can reduce noise to avoid saturation of the feedback system. This method is intuitive and easy to apply to actual storage rings. We discuss several examples of feedback with FIR filters obtained with this method, including the analysis of the stability of the feedback with FIR filters to show the available shortest damping time, and the discussion for the reduction of noise with those FIR filters.

I. INTRODUCTION

A feedback system for transverse betatron oscillation or longitudinal synchrotron oscillation of a storage ring is an effective device for suppression of beam instabilities that limit the current and the quality of the stored beam. Moreover, the feedback system can rapidly damp beam oscillations excited by injection perturbations [1, 2] that are harmful to user experiments at top-up operation of light source storage rings. Also this system is discussed as a device to suppress beam instabilities at energy recovery linacs [3]. The feedback system detects transverse or longitudinal positions of a beam, processes the position data to create a kick signal, and adds transverse or longitudinal kick to the beam to damp the oscillations of the beam. Recent feedback systems [4–44] employ digital signal processing and most of them use finite impulse response (FIR) filters as the algorithm for the digital signal processing. Because of their simplicity, FIR filters are used in bunch-by-bunch feedback systems that must process the beam position data at the bunch rate of hundreds of Megahertz within hundreds of nanoseconds.

In this study, we propose single-loop multi-dimensional feedback systems, in which the feedback uses a single position signal and a single kick signal to control the beam oscillations multi-dimensionally. For the calculation of the coefficients of FIR filters for such feedback scheme, we propose the time domain least square fitting method (TDLSF method) which can calculate the coefficients of FIR filters with arbitrary large number of taps. Such FIR filters can suppress noise to avoid the saturation of the feedback system. Also the TDLSF method is intuitive and, thus is easy to apply to actual storage rings. The basic concept of the TDLSF method is briefly described in Ref. [28] by the author; we will discuss the detail in this study. The discussion of FIR filters for feedback including the TDLSF method is in Ref. [45], for example.

Single-loop two-dimensional horizontal and vertical bunch-by-bunch feedback systems based on the scheme have been successfully tested or are in operation in several storage rings [30, 31, 34–37] with high-performance feedback processors [29] which are necessary to process the many taps FIR filters required for such single-loop multi-dimensional feedback systems. The coefficients of FIR filters for those systems are calculated by the TDLSF method. In addition, the TDLSF method is also employed at the HLS ring [38] and considered at the APS ring [40].

To control the longitudinal motion, we can use a change in the circumference of a ring produced by a kick at a dispersive section [46]. Based on this concept, several schemes for single-loop horizontal-longitudinal feedback have already been proposed by Chao et al. [47]. However, they did not show the possibility of the scheme of longitudinal feedback with a transverse feedback system at a dispersive section, in which a transverse position and a transverse kick are used as the input and the output of the feedback, respectively. Contrary to their result, we show that such a system can be realized using a digital signal processing scheme with an FIR filter, and we propose a single-loop three-dimensional feedback system that can simultaneously control horizontal, vertical and longitudinal oscillations. First, we describe the TDLSF method and then we discuss single-loop multi-dimensional feedback with FIR filters obtained with this method.

II. TIME DOMAIN LEAST SQUARE FITTING METHOD

A. Position and Kick for Feedback

We will discuss FIR filters for feedback systems. An FIR filter has a form of

$$y[n] = \sum_{k=0}^N a_k x_{n-k} \quad (1)$$

where x_k is the k -th input data, $y[n]$ is the n -th output data, a_k is the k -th coefficient of the FIR filter, and the number of input data, $N + 1$, is called the number of taps. For feedback systems, the input x_k is proportional to the measured beam position data at the k -th turn and the output $y[n]$ is proportional to the kick on the beam at the n -th turn as shown in Fig. 1.

We propose the TDLSF method to calculate the coefficients a_k of the FIR filter for feedback. The position of a beam at the k -th turn, $x[k]$, is produced by the betatron and/or synchrotron oscillations of the beam and has the form of

$$x[k] = A^{(0)} \cos \left(\Delta_k^{(0)} + \psi^{(0)} \right) + \sum_{m=1}^M A^{(m)} \cos \left((1 + \Delta^{(m)}) \phi_k^{(m)} + \psi^{(m)} \right) \quad (2)$$

where M is the number of oscillations of the beam and the superscript (m) specifies these oscillations; $A^{(m)}$ and $\psi^{(m)}$ are the amplitudes and the offset phases, respectively; $\phi_k^{(m)}$ and $(1 + \Delta^{(m)}) \phi_k^{(m)}$ are the assumed and actual phase advances at the k -th turn, respectively;

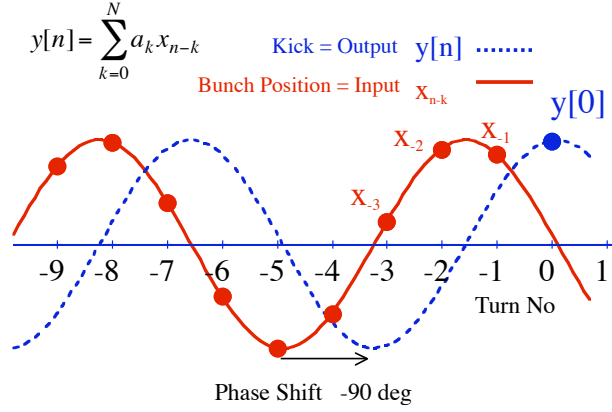


FIG. 1: An FIR filter for feedback on a storage ring. The filter produces a kick signal $y[n]$ (dotted line) turn-by-turn from the history of turn-by-turn beam position data x_k (solid line). The figure illustrates transverse feedback with a beam position monitor and a kicker placed at the same location. In such a case, the required phase shift between the beam position and the kick is -90 deg.

and $\Delta_k^{(0)}$ is the small phase change that represents the frequency response in the vicinity of DC.

By defining

$$P^{(m)} = A^{(m)} \cos \psi^{(m)} \quad (3)$$

$$Q^{(m)} = -A^{(m)} \sin \psi^{(m)}, \quad (4)$$

we can rewrite Eq. (2) as

$$\begin{aligned}
 x[k] = & P^{(0)} \cos \Delta_k^{(0)} + Q^{(0)} \sin \Delta_k^{(0)} \\
 & + \sum_{m=1}^M \left[P^{(m)} \cos \left((1 + \Delta^{(m)}) \phi_k^{(m)} \right) + Q^{(m)} \sin \left((1 + \Delta^{(m)}) \phi_k^{(m)} \right) \right]. \quad (5)
 \end{aligned}$$

We assume that the shift of the actual phase advances from the assumed phase advances are small as

$$|\Delta_k^{(0)}| \ll 1 \quad (6)$$

$$|\Delta^{(m)} \phi_k^{(m)}| \ll 1. \quad (7)$$

For the definition of $\Delta_k^{(0)}$ in Eq. (5), we have an ambiguity and we can set $\Delta_k^{(0)} = k\Delta^{(0)}$.

Then we can express the first two terms of the R.H.S. of Eq. (5) as

$$P^{(0)} \cos \Delta_k^{(0)} + Q^{(0)} \sin \Delta_k^{(0)} \simeq P^{(0)} + Q^{(0)} \Delta^{(0)} k = P_0^{(0)} + Q_1^{(0)} k \quad (8)$$

where we define

$$P_0^{(0)} = P^{(0)} \quad (9)$$

$$Q_1^{(0)} = Q^{(0)} \Delta^{(0)}. \quad (10)$$

With the assumption in Eq. (7), we can expand the other terms on the R.H.S. of Eq. (5) as

$$P^{(m)} \cos(1 + \Delta^{(m)}) \phi_k^{(m)} \simeq P_0^{(m)} \cos \phi_k^{(m)} + P_1^{(m)} \phi_k^{(m)} \sin \phi_k^{(m)} \quad (11)$$

$$Q^{(m)} \sin(1 + \Delta^{(m)}) \phi_k^{(m)} \simeq Q_0^{(m)} \cos \phi_k^{(m)} + Q_1^{(m)} \phi_k^{(m)} \cos \phi_k^{(m)} \quad (12)$$

where we define

$$P_0^{(m)} = P^{(m)} \quad (13)$$

$$P_1^{(m)} = -P^{(m)} \Delta^{(m)} \quad (14)$$

$$Q_0^{(m)} = Q^{(m)} \quad (15)$$

$$Q_1^{(m)} = Q^{(m)} \Delta^{(m)}. \quad (16)$$

Now, Eq. (5) can be expressed with them as

$$\begin{aligned} x[k] = & P_0^{(0)} + Q_1^{(0)} k \\ & + \sum_{m=1}^M \left(P_0^{(m)} \cos \phi_k^{(m)} + P_1^{(m)} \phi_k^{(m)} \sin \phi_k^{(m)} + Q_0^{(m)} \sin \phi_k^{(m)} + Q_1^{(m)} \phi_k^{(m)} \cos \phi_k^{(m)} \right) \end{aligned} \quad (17)$$

with the assumption of Eqs. (6) and (7).

For the feedback, the output of FIR filters (Eq. (1)) with the input $x_k = x[k]$ in Eq. (5) should have the form of

$$\begin{aligned} y[k] = & G^{(0)} A^{(0)} \cos \left(\Delta_k^{(0)} + \psi^{(0)} \right) \\ & + \sum_{m=1}^M G^{(m)} A^{(m)} \cos \left((1 + \Delta^{(m)}) (\phi_k^{(m)} + \varphi^{(m)}) + \zeta^{(m)} \right) \end{aligned} \quad (18)$$

where $G^{(m)}$ and $\zeta^{(m)}$ are the required gain and phase shift for the feedback, respectively, and $\varphi^{(m)}$ and $(1 + \Delta^{(m)})\varphi^{(m)}$ are the assumed and actual phase advances from the beam position monitor (BPM) to the kicker, respectively. We assume that the shift of this phase, $\Delta^{(m)}\varphi^{(m)}$, is proportional to the shift of the phase advance, $\Delta^{(m)}\phi_k^{(m)}$. Without the loss of generality, we can assume that $k = 0$ and $\phi_0^{(m)} = 0$ at the current turn and obtain

$$y[0] = G^{(0)} A^{(0)} \cos \psi^{(0)} + \sum_{m=1}^M G^{(m)} A^{(m)} \cos \left((1 + \Delta^{(m)})\varphi^{(m)} + \zeta^{(m)} \right). \quad (19)$$

With the same treatment as for $x[k]$, we obtain

$$y[0] = G^{(0)} P_0^{(0)} + \sum_{m=1}^M G^{(m)} \left(P_0^{(m)} \cos \zeta^{(m)} + P_1^{(m)} \varphi^{(m)} \sin \zeta^{(m)} + Q_0^{(m)} \sin \zeta^{(m)} + Q_1^{(m)} \varphi^{(m)} \cos \zeta^{(m)} \right). \quad (20)$$

Now we need to find an FIR filter that connects $x[k]$ in Eq. (17) and $y[0]$ in Eq. (20) with the required values of $G^{(m)}$, $\zeta^{(m)}$, $\phi_k^{(m)}$ and $\varphi^{(m)}$.

B. Least Square Fitting

$x[k]$ in Eq. (17) is the linear function of $P_0^{(m)}$, $Q_0^{(m)}$, $P_1^{(m)}$, and $Q_1^{(m)}$. If we assume that $P_0^{(m)}$, $Q_0^{(m)}$, $P_1^{(m)}$, and $Q_1^{(m)}$ are all independent of each other, we obtain $P_0^{(m)}$, $Q_0^{(m)}$, $P_1^{(m)}$, and $Q_1^{(m)}$ as linear functions of measured position data x_k by fitting the function $x[k]$ to x_k with a least square fitting method. As we can see in Eq. (20), $y[0]$ is also a linear function of $P_0^{(m)}$, $Q_0^{(m)}$, $P_1^{(m)}$, and $Q_1^{(m)}$. Thus, we can represent $y[0]$ as a linear function of x_k as in Eq. (1) and the coefficients of x_k are coefficients of the required FIR filter.

In reality, the parameters $P_0^{(m)}$, $Q_0^{(m)}$, $P_1^{(m)}$, and $Q_1^{(m)}$ are not independent as shown in Eqs. (13) to (16). However, if the position data x_k is that of a sinusoidal oscillation, the values of $P_0^{(m)}$, $Q_0^{(m)}$, $P_1^{(m)}$, and $Q_1^{(m)}$ obtained with this scheme automatically fulfill the relationships in Eqs. (13) to (16) in the vicinity of assumed phase advances $\phi_k^{(m)}$ where Eq. (7) is valid. In following examples, we will see the FIR filters obtained with this method have the expected frequency responses.

Applying the least square fitting method to fit $x[k]$ to x_k , we obtain

$$\frac{\partial S}{\partial P_i^{(m)}} = \frac{\partial S}{\partial Q_i^{(m)}} = 0 \quad (21)$$

$$i = 0, 1 \text{ and } m = 0, 1, 2, \dots, M \quad (22)$$

for

$$S = \sum_{k=0}^N (x[-k] - x_{-k})^2, \quad (23)$$

and Eq. (21) can be rewritten as

$$\sum_{k=0}^N \frac{\partial x[-k]}{\partial P_i^{(m)}} x[-k] = \sum_{k=0}^N \frac{\partial x[-k]}{\partial P_i^{(m)}} x_{-k} \quad (24)$$

$$\sum_{k=0}^N \frac{\partial x[-k]}{\partial Q_i^{(m)}} x[-k] = \sum_{k=0}^N \frac{\partial x[-k]}{\partial Q_i^{(m)}} x_{-k}. \quad (25)$$

Applying $x[k]$ in Eq. (17) to the above equations, we obtain a matrix equation:

$$CC^T \mathbf{v} = C\mathbf{x} \quad (26)$$

where we define vectors \mathbf{v} and \mathbf{x} , and a matrix C as

$$\mathbf{v} = \begin{pmatrix} P_0^{(0)} \\ Q_1^{(0)} \\ P_0^{(1)} \\ Q_0^{(1)} \\ P_1^{(1)} \\ Q_1^{(1)} \\ P_0^{(2)} \\ Q_0^{(2)} \\ P_1^{(2)} \\ Q_1^{(2)} \\ \vdots \end{pmatrix}, \quad \mathbf{x} = \begin{pmatrix} x_0 \\ x_{-1} \\ x_{-2} \\ x_{-3} \\ \vdots \\ x_{-N} \end{pmatrix}, \quad (27)$$

$$C = \begin{pmatrix} 1 & 1 & 1 & \dots & 1 \\ 0 & -1 & -2 & \dots & -N \\ C_0^{(1)} & C_{-1}^{(1)} & C_{-2}^{(1)} & \dots & C_{-N}^{(1)} \\ S_0^{(1)} & S_{-1}^{(1)} & S_{-2}^{(1)} & \dots & S_{-N}^{(1)} \\ \phi_0^{(1)} S_0^{(1)} & \phi_{-1}^{(1)} S_{-1}^{(1)} & \phi_{-2}^{(1)} S_{-2}^{(1)} & \dots & \phi_{-N}^{(1)} S_{-N}^{(1)} \\ \phi_0^{(1)} C_0^{(1)} & \phi_{-1}^{(1)} C_{-1}^{(1)} & \phi_{-2}^{(1)} C_{-2}^{(1)} & \dots & \phi_{-N}^{(1)} C_{-N}^{(1)} \\ C_0^{(2)} & C_{-1}^{(2)} & C_{-2}^{(2)} & \dots & C_{-N}^{(2)} \\ S_0^{(2)} & S_{-1}^{(2)} & S_{-2}^{(2)} & \dots & S_{-N}^{(2)} \\ \phi_0^{(2)} S_0^{(2)} & \phi_{-1}^{(2)} S_{-1}^{(2)} & \phi_{-2}^{(2)} S_{-2}^{(2)} & \dots & \phi_{-N}^{(2)} S_{-N}^{(2)} \\ \phi_0^{(2)} C_0^{(2)} & \phi_{-1}^{(2)} C_{-1}^{(2)} & \phi_{-2}^{(2)} C_{-2}^{(2)} & \dots & \phi_{-N}^{(2)} C_{-N}^{(2)} \\ & & \vdots & & \end{pmatrix}, \quad (28)$$

respectively, and

$$C_k^{(m)} = \cos \phi_k^{(m)} \quad (29)$$

$$S_k^{(m)} = \sin \phi_k^{(m)}. \quad (30)$$

The formal solution of Eq. (26) is

$$\mathbf{v} = D\mathbf{x} \quad (31)$$

$$D = (CC^T)^{-1}C. \quad (32)$$

From Eq. (31), we obtain

$$P_0^{(0)} = \sum_{k=0}^N D_{1,k} x_{-k} \quad (33)$$

$$Q_1^{(0)} = \sum_{k=0}^N D_{2,k} x_{-k} \quad (34)$$

$$P_0^{(m)} = \sum_{k=0}^N D_{j_m,k} x_{-k} \quad (35)$$

$$Q_0^{(m)} = \sum_{k=0}^N D_{j_{m+1},k} x_{-k} \quad (36)$$

$$P_1^{(m)} = \sum_{k=0}^N D_{j_{m+2},k} x_{-k} \quad (37)$$

$$Q_1^{(m)} = \sum_{k=0}^N D_{j_{m+3},k} x_{-k} \quad (38)$$

where we define j_m so that the j_m -th, $(j_m + 1)$ -th, $(j_m + 2)$ -th and $(j_m + 3)$ -th components of the vector \mathbf{v} are $P_0^{(m)}$, $Q_0^{(m)}$, $P_1^{(m)}$ and $Q_1^{(m)}$, respectively.

Then, inserting these to $y[0]$ in Eq. (20), we can represent $y[0]$ as a linear function of x_k , or the form for an FIR filter as

$$y[0] = \sum_{k=0}^N a_k x_{-k} \quad (39)$$

$$a_k = G^{(0)} D_{1,k} + \sum_{m=1}^M G^{(m)} \left(D_{j_m,k} \cos \zeta^{(m)} + D_{j_m+2,k} \varphi^{(m)} \sin \zeta^{(m)} \right. \\ \left. + D_{j_m+1,k} \sin \zeta^{(m)} + D_{j_m+3,k} \varphi^{(m)} \cos \zeta^{(m)} \right). \quad (40)$$

Although we showed the case of first-order expansions on $\Delta^{(m)}$ in the above discussion, the extension to higher-order expansions on $\Delta^{(m)}$ is easy. In what follows, we define $O^{(m)}$ to show the order of the expansions on $\Delta^{(m)}$.

The required conditions for an FIR filter can be represented with assumed phase advances $\phi_k^{(m)}$, gains $G^{(m)}$, phase shifts $\zeta^{(m)}$, assumed phases from a BPM to a kicker $\varphi^{(m)}$, and orders $O^{(m)}$. The total number of constraints on the coefficients of the FIR filter is

$$N_c = \sum_{m=0}^M (1 + O^{(m)})(2 - \delta_{m,0}) \quad (41)$$

where $\delta_{m,0}$ comes from the fact that the frequency of $m = 0$ is zero where the phase advance $\zeta^{(0)}$ does not exist. The number of taps must be greater than or equal to N_c .

C. Discussion

We will discuss the FIR filter obtained by the TDLSF method and define several parameters for later discussion. First, we will show the behavior of large number tap FIR filters obtained by the TDLSF method. If the input data has the form of

$$x_k = \sum_{m'=1}^{M'} \left(P^{(m')} \cos \phi_k^{(m')} + Q^{(m')} \sin \phi_k^{(m')} \right) \quad (42)$$

where $\phi_k^{(m')}(m' = 1, 2, \dots, M')$ is far from the target phase advances $\phi_k^{(m)}(m = 0, 1, 2, \dots, M)$. If we assume that N is large so enough as $\phi_N^{(m')} - \phi_N^{(m)} \gg 2\pi$ and

$\phi_N^{(m')} \gg 2\pi$, then we can use the following approximations:

$$\frac{1}{N} \sum_{k=0}^N C_{-k}^{(m')} \sim \frac{1}{N} \sum_{k=0}^N S_{-k}^{(m')} \sim 0 \quad (43)$$

$$\frac{1}{N} \sum_{k=0}^N k C_{-k}^{(m')} \sim \frac{1}{N} \sum_{k=0}^N k S_{-k}^{(m')} \sim 0 \quad (44)$$

$$\frac{1}{N} \sum_{k=0}^N C_{-k}^{(m)} C_{-k}^{(m')} \sim \frac{1}{N} \sum_{k=0}^N S_{-k}^{(m)} S_{-k}^{(m')} \sim 0 \quad (45)$$

$$\frac{1}{N} \sum_{k=0}^N C_{-k}^{(m)} S_{-k}^{(m')} \sim \frac{1}{N} \sum_{k=0}^N S_{-k}^{(m)} C_{-k}^{(m')} \sim 0 \quad (46)$$

$$\frac{1}{N} \sum_{k=0}^N \phi_k^{(m)} C_{-k}^{(m)} C_{-k}^{(m')} \sim \frac{1}{N} \sum_{k=0}^N \phi_k^{(m)} S_{-k}^{(m)} S_{-k}^{(m')} \sim 0 \quad (47)$$

$$\frac{1}{N} \sum_{k=0}^N \phi_k^{(m)} C_{-k}^{(m)} S_{-k}^{(m')} \sim \frac{1}{N} \sum_{k=0}^N \phi_k^{(m)} S_{-k}^{(m)} C_{-k}^{(m')} \sim 0 \quad (48)$$

where we define

$$C_k^{(m)} = \cos \phi_k^{(m)} \quad (49)$$

$$S_k^{(m)} = \sin \phi_k^{(m)}. \quad (50)$$

Then, from Eqs. (31) and (32) with the above approximations, we obtain

$$\mathbf{v} = D\mathbf{x} = 0, \quad (51)$$

or $P_0^{(0)} = Q_1^{(0)} = 0$ and $P_0^{(m)} = Q_0^{(m)} = P_1^{(m)} = Q_1^{(m)} = 0$ for $m \neq 0$. Thus, we obtain the output of the FIR filter $y[n] = 0$ for the input of x_k in Eq. (42). This results shows that we can reduce the gain at phase advances other than the target phase advances just by increasing the number of taps and this is the advantage of the TDLSF method. However, the regions where the frequency response is insensitive to the tune shift around the target tunes become narrower as N increases because the assumption $\Delta^{(m)} \phi_{-N}^{(m)} \ll 1$ based on Eq. (7) breaks even for small $\Delta^{(m)}$ for large N .

When the beam position is measured turn-by-turn as in a storage ring, we can set the assumed phase advances to be

$$\phi_k^{(m)} = 2\pi \Delta \nu^{(m)} k \quad (52)$$

where $\Delta\nu^{(m)}$ are the fractional part of the assumed tunes of betatron or synchrotron oscillations. For this case, we can write the required condition to calculate the FIR filter with the TDLSF method as a set of parameters of

$$\{(G^{(0)}, O^{(0)}), \{(\Delta\nu^{(m)}, G^{(m)}, \zeta^{(m)}, \varphi^{(m)}, O^{(m)}) | m = 1, 2, 3, \dots, M\}\}. \quad (53)$$

In the following sections, we call $\Delta\nu^{(m)}$ the "target tunes" of an FIR filter. In the examples shown in later sections, we assume that a BPM and a kicker are placed at the same location ($\varphi^{(m)} = 0$) and, in such cases, we omit $\varphi^{(m)}$ in the above condition. With the definition of k in Eq. (52), the number of taps is the number of non-zero coefficients of a_k in this case. We need to set $a_k = 0$ for $k \leq n - 1$ for n -turn delay. Here, we use "n-turn delay" to show how many turns for the kick signal from the feedback to catch the beam at the kicker after the position measurements of which position data is used to create this kick.

If the input and output of the FIR filter, $x[n]$ and $y[n]$, respectively, are the oscillations with the tune $\Delta\nu$, then, we can set

$$x[n] = \Re[\tilde{x}e^{in2\pi\Delta\nu}] \quad (54)$$

$$y[n] = \Re[\tilde{y}e^{in2\pi\Delta\nu}], \quad (55)$$

and we call \tilde{x} and \tilde{y} the complex amplitude of $x[n]$ and $y[n]$. For the such input and output, we have frequency response of the FIR filter in Eq. (1) as

$$\tilde{y} = \tilde{G}(\Delta\nu)\tilde{x} \quad (56)$$

$$\tilde{G}(\Delta\nu) = G(\Delta\nu)e^{i\zeta(\Delta\nu)} = \sum_{k=0}^N a_k e^{-ik2\pi\Delta\nu} \quad (57)$$

where the gain and the phase of the FIR filter are $G(\Delta\nu) = |\tilde{G}(\Delta\nu)|$ and $\zeta(\Delta\nu) = \arg[\tilde{G}(\Delta\nu)]$, respectively.

In some cases, noise in the output of FIR filters saturates a power amplifier for a kicker or prevents us to observe the beam motion. Such noise is usually produced in front-end circuits and passes through the FIR filter. The FIR filter for the feedback can be used also for the filter of the noise. If we assume that the spectrum of the noise in the input to the FIR filter is white, the noise power in the output of the FIR filter is proportional to

$$P = \int_0^1 |\tilde{G}(\Delta\nu)|^2 d(\Delta\nu) = \int_0^1 \left| \sum_{k=0}^N a_k e^{-ik2\pi\Delta\nu} \right|^2 d(\Delta\nu) = \sum_{k=0}^N a_k^2 \quad (58)$$

where $|\tilde{G}(\Delta\nu)|$ is the frequency response of the gain of the filter in Eq. (57). To reduce the noise in the output of the filter, we need to reduce the gain at tunes other than the target tunes. As shown above, the TDLSF method can produce any large number of tap FIR filters without additional constraints and such FIR filters have small gain at tunes other than target tunes, which make the feedback low noise.

In Appendix VII, we discuss the parameters to be specified for the TDLSF method for the case with localized sources of tune shifts. And a comparison of the TDLSF method with a frequency domain approach will be made in Appendix VIII.

III. ONE-DIMENSIONAL FEEDBACK

A. Transverse Feedback

1. FIR Filter

We applied the TDLSF method to obtain FIR filters for the one-dimensional transverse feedback systems for horizontal and vertical directions at the SPring-8 storage ring [28].

The schemes of the transverse feedback with FIR filters are summarized in Appendix IX A; we choose the transverse position of the beam as the input to the feedback and the transverse kick as the output. Then we set $K \neq 0$ and $F = 0$ in Eq. (119) in Appendix IX A and the number of oscillations M in Eq. (2) to one.

In the discussions in this subsection, we assume that FIR filters fulfill the DC condition:

$$(G^{(0)}, O^{(0)}) = (0, 0). \quad (59)$$

With this condition, FIR filters suppress DC offset contamination in a position signal. The DC offset is produced by several effects: closed orbit distortions (COD); unequal bunch signal shapes from BPM electrodes; and reflection at cable connections. The DC offset drives the kicker if we do not suppress it with the signal processing.

In the SPring-8 storage ring, the horizontal and vertical fractional tunes are 0.15 and 0.35, respectively, and the BPM and the kicker are placed at the same location. Then, from Eq. (129), the required phase shift is -90 deg. ($\zeta = -\frac{\pi}{2}$) as in the case of Fig. 1. The

conditions for the FIR filters are

$$(\Delta\nu, G, \zeta, O) = \left(0.15, 1, -\frac{\pi}{2}, 1\right) \quad (60)$$

for the horizontal feedback and

$$(\Delta\nu, G, \zeta, O) = \left(0.35, 1, -\frac{\pi}{2}, 1\right) \quad (61)$$

for vertical feedback and we use the 1st order expansion with $\Delta\nu$. The gain of the FIR filters are normalized to the gain at the each target tune. With the above conditions and Eq. (59), the required minimum number of taps (Eq. (41)) is 5 for both directions.

We use 9-tap FIR filters with the position data at nine previous turns ($k = -1, -2, -3, \dots, -9$), where we use one-turn delay: the coefficient of the 0th turn to zero ($a_0 = 0$). The calculated coefficients of the FIR filters with the TDLSF method are shown in Fig. 2 and the frequency responses of those filters are shown in Fig. 3.

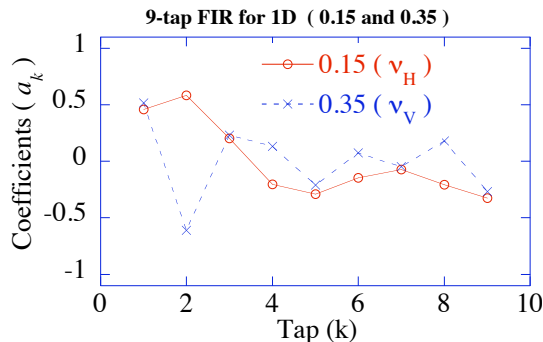


FIG. 2: Coefficients of the 9-tap FIR filters for horizontal and vertical one-dimensional transverse feedback. The horizontal and vertical target tunes are 0.15 and 0.35, respectively

For comparison, we show the frequency response of a possible 5-tap FIR filter ($k = -1, -3, -5, -7, -9$) in Fig. 4. The coefficients of the 5-tap FIR filters for horizontal and vertical feedback are coincidentally identical in this case. The 5-tap FIR filter have larger gain than 9-tap filters at tunes other than target tunes because of one more passband produced by aliasing effect, hence the noise that passes through the 5-tap FIR filter is larger than that of the 9-tap filters as discussed in Section II C. We also show the frequency responses of 15-tap FIR filters with every single turn position data in Fig. 5. The gain at tunes other than the target tune is smaller than the 9-tap filters, however, the frequency

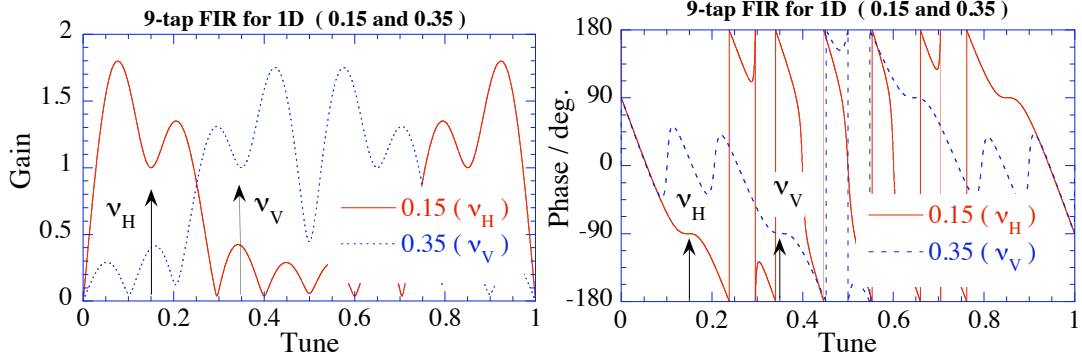


FIG. 3: Frequency responses of gain and phase of the 9-tap FIR filters for horizontal and vertical one-dimensional transverse feedback. The horizontal and vertical target tunes are 0.15 and 0.35, respectively.

response of the gain and phase are more sensitive to the tune shift and the acceptance to the tune shift is narrower as we mentioned in Section II B. To fulfill the requirements of acceptance, stability and noise of the feedback, we need to compare several FIR filters with different values of N and $O^{(m)}$, and sometimes we need to adjust the frequency response by shifting the target tune itself. Adding to the above discussion about transverse motion, if

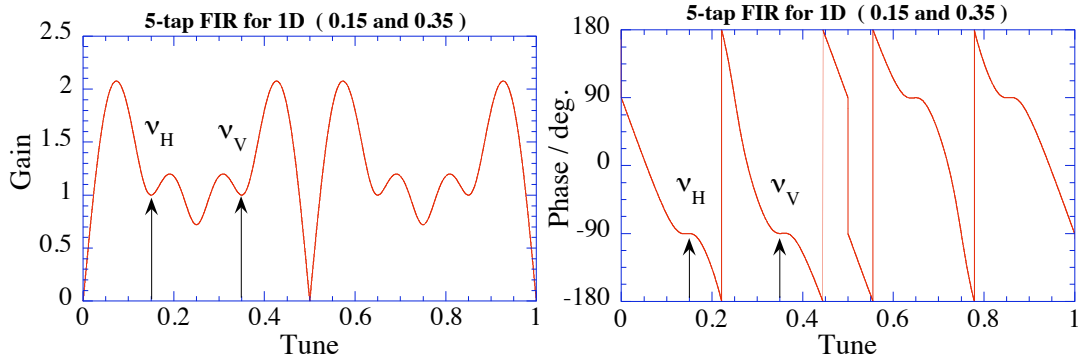


FIG. 4: Frequency responses of gain and phase of the 5-tap FIR filters for one-dimensional transverse feedback with the position data for 1st, 3rd, 5th, 7th and 9th previous turns. The FIR filters for horizontal and vertical are coincidentally identical in this case.

a BPM and a kicker for feedback are placed in dispersive sections, such feedback also affects the longitudinal motion and the consideration on it is necessary as in Section V.

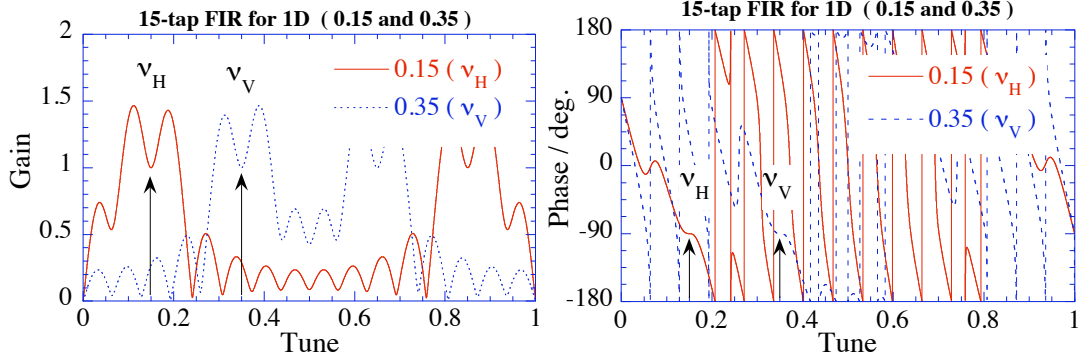


FIG. 5: Frequency responses of gain and phase of the 15-tap FIR filters for one-dimensional transverse feedback with the position data of every single turn. The gain at tunes other than the target tune is smaller than the 9-tap filter, however, the variation of the gain and phase to the tune shift is larger and the width of the tune acceptance is narrower.

2. Stability

Following the discussion in Appendix IX C, we will analyze the stability of the horizontal and vertical feedback. For the horizontal feedback for the target tune $\Delta\nu_0 = 0.15$, the tunes of 0.056 and 0.24 are on the boundary of the stable region because the phases of the FIR filter at those tunes are -180 deg. and 0 deg., respectively, as seen in Fig. 3. These are the proper phases to drive the tune shift from 0.15 to 0.056 and 0.24, respectively, as the discussion in Appendix IX C.

From Eq. (162) in Appendix IX C, the frequency response of the FIR filter is proportional to

$$\tilde{G}(\Delta\nu) = \frac{1}{2}\beta\tilde{K}(\Delta\nu)\sin\phi_0 \quad (62)$$

where $\phi_0 = 2\pi\Delta\nu_0$, and is shown in Fig. 3 with the normalization of the gain to the value at the target tune.

For $\Delta\nu_1 = 0.056$, we obtain $\left|\tilde{G}(\Delta\nu_0)/\tilde{G}(\Delta\nu_1)\right| = 1/1.65$ from Fig. 3 and the maximum stable feedback damping rate per turn from Eq. (166) is

$$|\phi_I| = \left|\frac{\cos\phi_1 - \cos\phi_0}{\sin\phi_0}\right| \left|\frac{\tilde{G}(\Delta\nu_0)}{\tilde{G}(\Delta\nu_1)}\right| = 0.43 \times 1/1.65 = 1/3.8 \quad (63)$$

where we set $\phi_1 = 2\pi\Delta\nu_1$. For $\Delta\nu_1 = 0.24$, we obtain $\left|\tilde{G}(\Delta\nu_0)/\tilde{G}(\Delta\nu_1)\right| = 1/1.1$ and $|\phi_I| = 1/1.7$ which is larger than that for $\Delta\nu_1 = 0.056$. From those results, the maximum stable

feedback damping rate is limited by the boundary at tune 0.056 and $|\phi_I| = T_0/\tau_{FB} = 1/3.8$ or the shortest stable feedback damping time is $3.8T_0$ where T_0 is the revolution period of the ring.

A simulation was performed with Eq. (119) and the result is shown in Fig. 6, which shows the emergence and growth of the oscillation of $\Delta\nu = 0.0056$ after the 520th turn for the feedback damping time $3.6T_0$. The damping time $3.8T_0$ is the threshold of the instability because no growth of the oscillation of $\Delta\nu = 0.0056$ is seen with this feedback damping time and it is the shortest stable feedback damping time. This value agrees with the estimated value above. The growth rate by other effects is set to zero in this simulation.

The results of simulation with finite growth rates are shown in Fig. 7. The figure shows that the feedback with damping time $5T_0$ can suppress the growth of the growth time $6T_0$ and the feedback achieves a high damping rate at the target tune even with high feedback gain near the edge of stability.

For vertical feedback ($\Delta\nu_0 = 0.35$), the phase is 180 deg at the tune $\Delta\nu_1 = 0.45$ and the maximum stable feedback damping rate is $T_0/\tau_{FB} = -1/3.3$ and the simulation also shows $-1/3.3$.

B. Longitudinal Feedback

1. FIR Filter

We will discuss several candidates of FIR filters for longitudinal feedback of the SPring-8 storage ring. The schemes for longitudinal feedback are summarized in Appendix IX B; we choose the timing position τ as the input to the feedback and the energy kick U as the output. Then, we set $P \neq 0$ and $W = K = F = 0$ in Eqs. (138) and (139) in Appendix IX B.

The synchrotron tune of the SPring-8 ring is $\nu_s = 0.007$ and the required phase of an FIR filter for the damping is 90 deg. as shown in Eq. (152). We use the 2nd order expansion with the shift of the actual tune from the target tune to obtain wider acceptance to the tune shift. Thus, the condition for the FIR filter with these parameters is

$$(\Delta\nu, G, \zeta, O) = \left(0.007, 1, \frac{\pi}{2}, 2\right). \quad (64)$$

and we set $(G^{(0)}, O^{(0)}) = (0, 0)$ for DC.

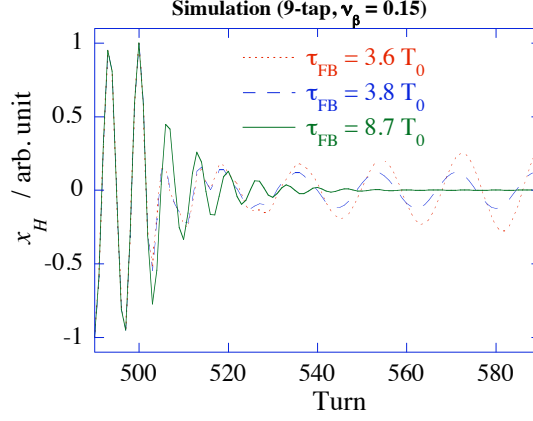


FIG. 6: Simulation result of horizontal feedback ($\Delta\nu_0 = 0.15$) with Eq. (119) for several feedback damping time: $3.6T_0$ (dotted line), $3.8T_0$ (dashed line), and $8.7T_0$ (solid line). With the damping time of $3.8T_0$ and $3.6T_0$, the oscillations of $\Delta\nu_1 = 0.056$ can be seen after the 520th turn.

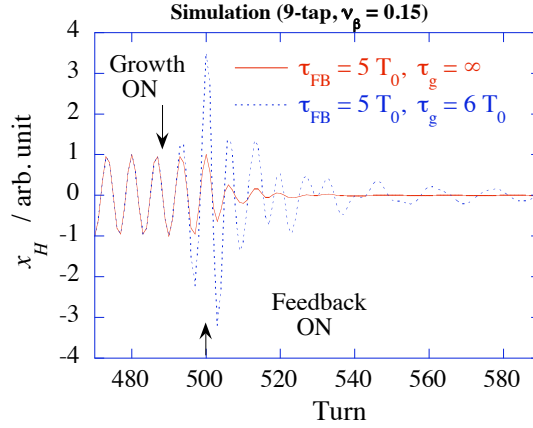


FIG. 7: Simulation result for horizontal feedback ($\Delta\nu_0 = 0.15$) with Eq. (119) with the growth of the oscillation of two growth times: ∞ (solid line) and $6T_0$ (dotted line). The feedback damping time is set to $5T_0$. The growth is turned on at the 490th turn and the feedback is turned on at the 500th turn.

For the tune of 0.007, we need to treat the position data during more than one hundred turns to reduce gain at tunes other than the target tune. If we directly apply FIR filters for that number of taps, the required resources of digital signal processing devices are enormous, much beyond the capacity of current devices; we must use a scheme to reduce the amount of position data. For such scheme, we will discuss downsampling and decimation which are easy to implement to digital signal processing devices by programming.

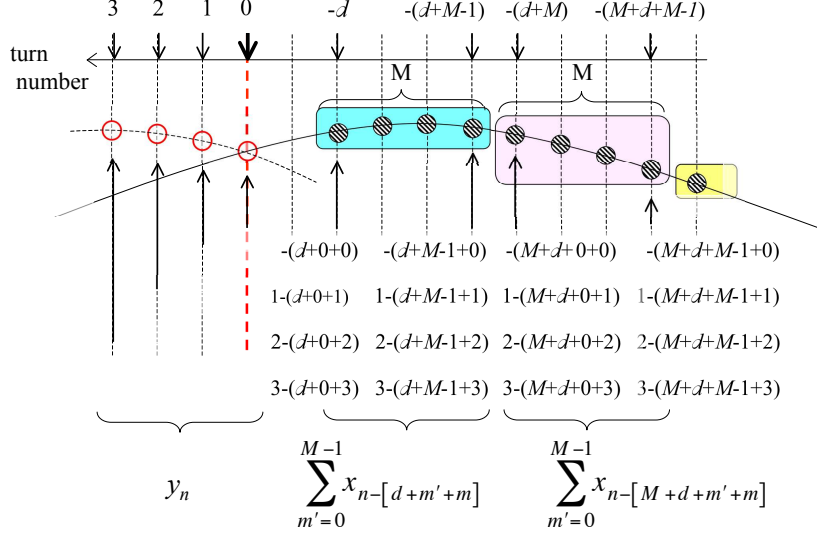


FIG. 8: Scheme of decimation. The position data of a bunch during M turns (hatched circles) are averaged to form an input datum (square boxes) to an FIR filter. From the output data (non-hatched circles), the input data timing to the filter changes turn-by-turn as in Eq. (66).

With downsampling, an FIR filter samples every M turn position data to reduce the number of taps. However, such a filter with a large M has many passbands other than the target tunes by aliasing effect and passes noise in those passbands, as we already saw in the responses of the 5-tap filters ($M=2$) for transverse feedback in Fig. 4.

With decimation, the position data of a bunch during M turns are averaged to form an input datum to an FIR filter as shown in Fig. 8. We call M the factor of decimation. Compared with downsampling, higher-frequency noise is averaged out by decimation and the passbands seen in the downsampling FIR filters are suppressed. However, M should be sufficiently small for the decimation not to averaged out the oscillation itself.

We will discuss the following FIR filters: a 256-tap FIR filter with the data of every single turn ($M = 1$), a 16-tap FIR filter with decimation by a factor of 16 ($M = 16$), and an 8-tap FIR filter with decimation by a factor of 32 ($M = 32$).

Since the TDLSF method cannot handle decimation directly, decimation is applied on the coefficients of the downsampling 16-tap and 8-tap FIR filters, obtained with the TDLSF method. The downsampling FIR filters have the form of

$$y_{DS}^{(M)}[n] = \sum_{k=1}^N a_k x_{n-(kM+d-1)}, \quad (65)$$

where d indicates a d -turn delay. The FIR filter with decimation is

$$\begin{aligned} y_{deci}^{(M)}[n] &= y^{(M,m)}[n] \\ m &= n \pmod{M} \end{aligned} \quad (66)$$

where

$$y^{(M,m)}[n] = \sum_{k=1}^N a_k \frac{1}{M} \sum_{m'=0}^{M-1} x_{n-[(k-1)M+d+m'+m]} \quad (67)$$

for $m = 0, 1, 2, \dots, M - 1$.

For comparison, we will make an FIR filter by averaging $y^{(M,m)}[n]$ over m as

$$\bar{y}^{(M)}[n] = \frac{1}{M} \sum_{m=0}^{M-1} y^{(M,m)}[n] = \frac{1}{M^2} \sum_{k=1}^N a_k \sum_{m=0}^{M-1} \sum_{m'=0}^{M-1} x_{n-[(k-1)M+d+m'+m]}. \quad (68)$$

This form of $\bar{y}^{(M)}[n]$ shows that it is a linear interpolation of the FIR filter of $y_{DS}^{(M)}[n]$. By decimation, a bunch is kicked by a different FIR filter $y^{(M,m)}[n]$ as the turn number n changes. However, the motion of the oscillation is much slower in the timescale of M turns, therefore, the effect of those kicks on the bunch is averaged by m . Thus, we can expect that the effect of those kicks is well approximated by the effect of the FIR filter $\bar{y}^{(M)}[n]$.

The coefficients of $y_{DS}^{(M)}[n]$ and $\bar{y}^{(M)}[n]$ for the conditions of Eq. (64) and $(G^{(0)}, O^{(0)}) = (0, 0)$ with one-turn delay ($d = 1$) are shown in Fig. 9.

The results of the simulation with the FIR filters $y_{deci}^{(M)}[n]$ and $\bar{y}^{(M)}[n]$ based on Eq. (138) and Eq. (139) are shown in Fig. 10. We can see the good agreement between the results of these two FIR filters and $\bar{y}^{(M)}[n]$ are the good approximation of the FIR filters with decimation, $y_{deci}^{(M)}[n]$, as expected. The frequency responses of $\bar{y}^{(M)}[n]$ at the vicinity of the target tune $\Delta\nu = 0.007$ are shown in Fig. 11 and shows a tune acceptance as large as that of a 12-tap IIR filter discussed in Ref. [48]. In Fig. 11, the gain or the feedback damping rate at the target tune $\Delta\nu = 0.007$ are reduced from the gain specified by the condition for the FIR filters in Eq. (64), as the increase of the decimation factor M . This gain reduction is caused by the averaging effect of the decimation and the actual damping time of the beam is longer than that we expect from the condition Eq. (64). For the simulation in Fig. 10, this reduction of the gain is compensated and the damping time shown are the actual damping time.

The frequency responses of the gain of $y_{DS}^{(M)}[n]$ and $y^{(M,m)}[n]$ are shown in Fig. 12 and Fig. 13, respectively, and the P values in Section II C which represent the noise power are

TABLE I: Values for P in Eq. (58) for the FIR filters: $y_{DS}^{(M)}[n]$ and $y^{(M,m)}[n]$, with number of taps (N) and decimation factors (M).

N	M	P	
		$y_{DS}^{(M)}[n]$	$y^{(M,m)}[n]$
8	32	2.7	0.084
16	16	1.6	0.099
32	8	0.81	0.10
64	4	0.41	0.10
256	1	0.10	

listed in Table I. The filters $y^{(M,m)}[n]$ do not have passband peaks seen in the the frequency response of the gain of the downsampling FIR filters $y_{DS}^{(M)}[n]$ and the P values of $y^{(M,m)}[n]$ are M times smaller than those of $y_{DS}^{(M)}[n]$ and the noise is reduced with decimation.

In addition, in Fig. 10, we can see the emergence of an oscillation of tune 0.002 after the 1000th turn for the damping time $142T_0$. This oscillation is excited by the feedback itself, which we will discuss later in this section.

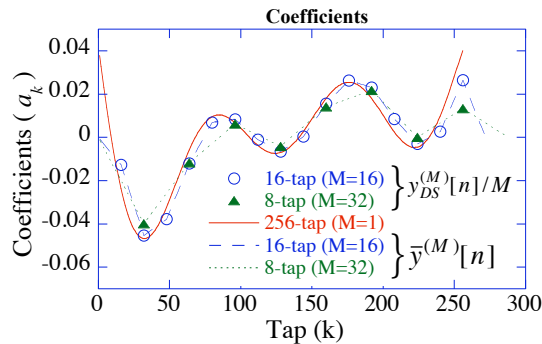


FIG. 9: The coefficients of the FIR filters of $y_{DS}^{(M)}[n]$ and $\bar{y}^{(M)}[n]$. $y_{DS}^{(M)}[n]$ of a 256-tap with $M=1$ (solid line); a 16-tap with $M=8$ (circles); and an 8-tap with $M=16$ (triangles), and $\bar{y}^{(M)}[n]$ of a 16-tap (dashed line) and an 8-tap (dotted line) are shown. The coefficients of $y_{DS}^{(M)}[n]$ are normalized by M .

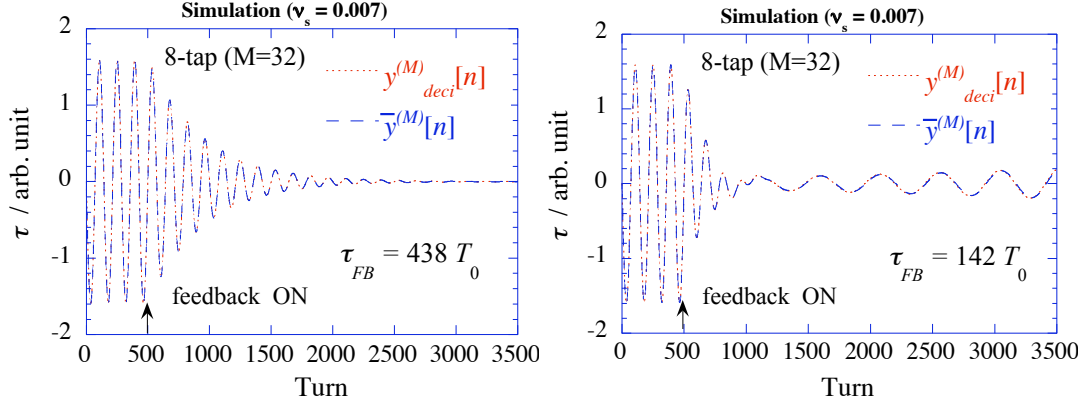


FIG. 10: Simulation result of longitudinal feedback with Eqs. (138) and (139) with 8-tap FIR filters with decimation by a factor 32: $y_{dec}^{(M=32)}[n]$ (dotted line) and $\bar{y}^{(M=32)}[n]$ (dashed line), with a actual feedback damping time of 438 turns ($\tau_{FB} = 438T_0$) and 142 turns ($\tau_{FB} = 142T_0$). The feedback is turned on at the 500th turn. The results of two filters agree well. The oscillation of the tune 0.002 is observed after the 1000th turn for the damping time $142T_0$, which is excited by the feedback itself.

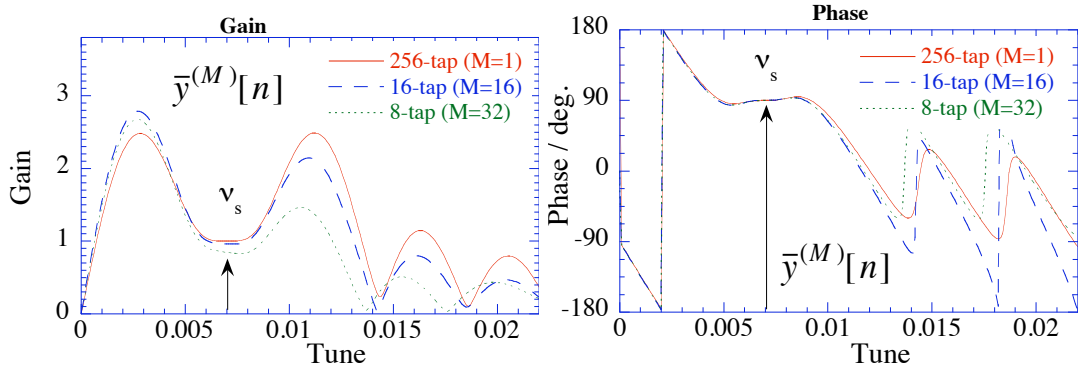


FIG. 11: Frequency responses of the gain and phase of the FIR filters $\bar{y}^{(M)}[n]$ in the vicinity of $\Delta\nu_0 = \nu_s$. A 256-tap with $M=1$ (solid line), a 16-tap with $M=16$ (dashed line), and an 8-tap with $M=32$ (dotted line) are shown.

2. Stability

We will analyze the stability of longitudinal feedback by following the discussion in Appendix IX C. From Eq. (167) in Appendix IX C, the frequency response of the FIR filter is

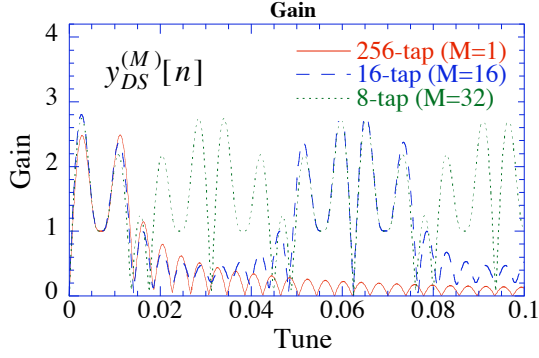


FIG. 12: Frequency responses of the gain of the downsampling FIR filters, $y_{DS}^{(M)}[n]$: a 256-tap with $M=1$ (solid line), a 16-tap with $M=16$ (dashed line), and an 8-tap with $M=32$ (dotted line). We can see many passbands other than the target tune ($\Delta\nu_0 = 0.007$) .

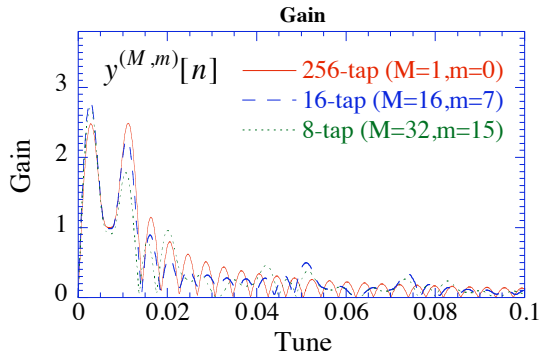


FIG. 13: Frequency responses of the gain of the FIR filters of $y^{(M,m)}[n]$: a 256-tap with $M=1$ (solid line), a 16-tap with $M=16$ (dashed line), and an 8-tap with $M=32$ (dotted line).

proportional to

$$\tilde{G} = \alpha T_0 \tilde{P}. \quad (69)$$

As examples, we take a 256-tap FIR filter $y_{deci}^{(M=256)}[n] = y_{DS}^{(M=256)}[n]$ and a 8-tap FIR filter with decimation $y_{deci}^{(M=32)}[n]$ for the tune $\Delta\nu_0 = 0.007$ ($\phi_0 = 0.044$). The frequency response of the 256-tap filter in Fig. 11 shows that the phase of the filter is 180 deg. and 0 deg. at $\Delta\nu_1 = 0.002$ ($\phi_1 = 0.013$) and $\Delta\nu_1 = 0.012$ ($\phi_1 = 0.075$), respectively, and those are the proper phase to drive the tune from $\Delta\nu_0$ to $\Delta\nu_1$ as shown in Appendix IX C. For $\Delta\nu_1 = 0.002$, we obtain $\left| \tilde{G}(\Delta\nu_0)/\tilde{G}(\Delta\nu_1) \right| = 1/2.2$ from Fig. 11 and, from Eq. (171), the

maximum stable damping rate per turn is

$$|\phi_I| = \left| \frac{\phi_1^2 - \phi_0^2}{2\phi_0} \right| \left| \frac{\tilde{G}(\Delta\nu_0)}{\tilde{G}(\Delta\nu_1)} \right| = 0.020 \times 1/2.2 = 1/111. \quad (70)$$

For $\Delta\nu_0 = 0.012$, we obtain $\left| \tilde{G}(\Delta\nu_0)/\tilde{G}(\Delta\nu_1) \right| = 1/2.3$ and $|\phi_I| = 1/54$ which is smaller than the value for $\Delta\nu_1 = 0.002$ and the shortest stable damping time with this FIR filter is $111T_0$ for $\Delta\nu_1 = 0.002$.

The simulation with Eqs. (138) and (139) shows that the oscillation is unstable for the damping time shorter than $\sim 114T_0$ at $\Delta\nu_1 = 0.002$ which is in agreement with the expected value above. The results for several feedback damping rates are shown in Fig. 14; the growth of the oscillation of $\Delta\nu_1 = 0.002$ can be seen after the 1000th turn for shorter damping times.

For the FIR filter with decimation $y_{deci}^{(M=32)}[n]$, we do not have definite frequency response and we use the frequency response of $\bar{y}^{(M=32)}$ in Fig. 11 instead. The phase of the filter is 180 deg. and 0 deg. at $\Delta\nu_1 = 0.002$ and $\Delta\nu_1 = 0.012$, respectively, and those are proper phase to drive such tune shift. For $\Delta\nu_1 = 0.002$, we obtain $\left| \tilde{G}(\Delta\nu_0)/\tilde{G}(\Delta\nu_1) \right| = 1/2.9$ and the maximum stable damping rate per turn is $|\phi_I| = 1/148$. For $\Delta\nu_1 = 0.012$, we have $\left| \tilde{G}(\Delta\nu_0)/\tilde{G}(\Delta\nu_1) \right| = 1/1.4$ and $|\phi_I| = 1/35$ which is smaller than the value for $\Delta\nu_1 = 0.002$, and the maximum stable damping rate per turn is $1/148$ or the shortest stable damping time is $148T_0$ at $\Delta\nu_1 = 0.002$. The simulation result with $y_{deci}^{(M=32)}[n]$ shows that the beam is unstable at $\Delta\nu_1 = 0.002$ for the damping time shorter than $148T_0$ as in the simulation result in Fig. 10 for the damping time $142T_0$.

C. Longitudinal Feedback by a Transverse Kick at Dispersion

In the schemes shown in Appendix IX B, if we choose a transverse kick at a dispersive section for the output of the feedback, we can control the revolution period, and the longitudinal feedback is possible using not an energy kicker (longitudinal kicker) but a transverse kicker. For the input to the feedback, we can use the timing of a bunch or the energy shift measured as a transverse position at a dispersive section. In the latter case, we can perform the feedback with the same setup as for the transverse feedback. However, we need to prepare an FIR filter of the band elimination at the horizontal tune [49] or the filter with proper gain and phase at the horizontal tune to control the horizontal motion.

We will show such an FIR filter in a later section.

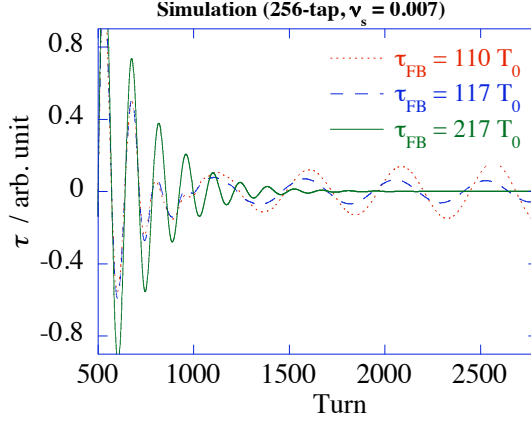


FIG. 14: Simulation result of longitudinal feedback with Eqs. (138) and (139) for a 256-tap FIR filter for $\Delta\nu_0 = 0.007$ at several feedback damping times ($\tau_{FB} = 110T_0$, $117T_0$, and $217T_0$): The oscillation of the tune 0.002 is observed after the 1000th turn for the feedback damping times of $110T_0$ and $117T_0$.

In such a scheme, the feedback system cannot distinguish oscillation due to the COD and the synchrotron oscillation through dispersion. If the COD oscillation exists, it excites the feedback and drives the longitudinal motion. If this is a serious problem, we have to use more BPMs to cancel the betatron motion signal by choosing the proper betatron phase relationship between them.

Also the advantage of the scheme of the control of longitudinal motion by transverse kick is that we can control the longitudinal motion of coasting beams because the frequency of the kick is much lower than the longitudinal kickers with RF cavities or striplines that are intrinsically high frequency devices for bunched beams.

IV. TWO-DIMENSIONAL TRANSVERSE FEEDBACK BY A SINGLE-LOOP

We propose single-loop two-dimensional transverse feedback with FIR filters. The advantages of this scheme is that one signal line, one processor, and one kicker are enough for two-dimensional feedback, which make the system easy to setup and tuning, and low in cost.

In longitudinal direction, the control of two oscillation of different tunes-a dipole and a quadrupole modes- are already achieved at DAFNE[18, 50] with a single loop by adjusting

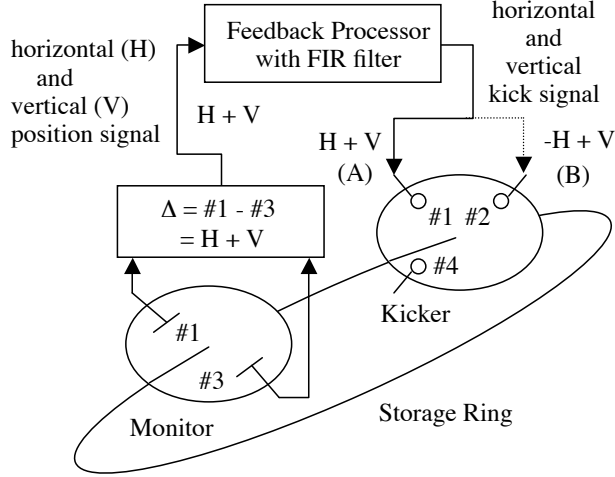


FIG. 15: Single-loop two-dimensional feedback. For the configuration between the pair of BPM electrodes and the kicker electrode, we have two choices: the case A (solid line) and the case B (dotted line). The same setup can be used for single-loop three-dimensional feedback which is described later in this study.

the response of an FIR filter at those tunes.

Using the BPM electrodes at skewed positions as shown in Fig. 15, we can detect the horizontal and vertical betatron oscillations with a single signal as

$$S_{in} = C_H x_H + C_V x_V \quad (71)$$

where x_H and x_V are the horizontal and vertical beam positions, respectively; C_H and C_V are the sensitivity of the BPM to horizontal and vertical positions, respectively. We use S_{in} as the input to the feedback. For the kicker, we use electrodes at skewed positions as shown in Fig. 15 and we can add a kick to the beam horizontally and vertically, by a single signal S_{out} from the feedback processor to the kicker as

$$\mathbf{R} = (D_H \hat{\mathbf{x}}_H + D_V \hat{\mathbf{x}}_V) S_{out} \quad (72)$$

where \mathbf{R} is the kick vector; $\hat{\mathbf{x}}_H$ and $\hat{\mathbf{x}}_V$ are the unit vectors for horizontal and vertical directions, respectively; and D_H and D_V are the kicker efficiencies to horizontal and vertical directions, respectively.

Thus, if we have an FIR filter that has proper gain and phase at the horizontal and vertical tunes, we can control those two-dimensional oscillations by a single signal, or single feedback loop. We will show such FIR filters calculated with the TDLSF method.

TABLE II: Transverse parameters of the Photon Factory ring at the BPM and the kicker. (H) and (V) indicate horizontal and vertical values, respectively.

Fractional betatron tunes	0.60 (H) / 0.28 (V)	
Betatron function / m	5.8 (H) / 5.8 (V)	
Ratio of sensitivity of BPM (C_H/C_V)	3	
Configuration	A	B
Ratio of kick strength (D_H/D_V)	1	-1

Single-loop two-dimensional transverse feedback systems with the scheme proposed here are in operation at Photon Factory [30, 31], Taiwan Light Source [34], and SOLEIL [37]. As an example, we consider the Photon Factory ring of which the transverse parameters are listed in Table II. As shown in Fig. 15, we have two choices in the configurations between the pair of BPM electrodes and the kicker electrode: A) The kicker electrode placed at #1, and B) The kicker electrode placed at #2. In case B, we must invert the direction of the horizontal kick compared to case A.

To obtain the same damping rate in the horizontal and vertical directions, we compensate the ratio of the position sensitivity of the BPM in horizontal and vertical by increasing the gain of the FIR filter at the vertical tune by a factor of $C_H/C_V = 3$ in Table II. The BPM and the kicker are placed at the same location. The required condition for the FIR filter is

$$\{(\Delta\nu^{(1)}, G^{(1)}, \zeta^{(1)}, O^{(1)}), (\Delta\nu^{(2)}, G^{(2)}, \zeta^{(2)}, O^{(2)})\} = \begin{cases} \{(0.60, 1, -\frac{\pi}{2}, O^{(1)}), (0.28, 3, -\frac{\pi}{2}, O^{(2)})\} & \text{for case A} \\ \{(0.60, 1, \frac{\pi}{2}, O^{(1)}), (0.28, 3, -\frac{\pi}{2}, O^{(2)})\} & \text{for case B} \end{cases} \quad (73)$$

where $O^{(1)}$, $O^{(2)}$ and the number of taps are tuning parameters to obtain wider tune acceptance and less noise, and the phase is flipped for the horizontal direction in case B. If we set $O^{(1)} = O^{(2)} = 1$, and $O^{(0)} = 0$ for DC, the required minimum number of taps of the FIR filter is 9. We assume that the feedback system kicks a beam with a one-turn delay: the coefficient of the 0th turn is zero ($a_0 = 0$).

The coefficients of a 9-tap FIR filter with the position data of nine previous turns ($k = 1, 2, 3, \dots, 9$) for cases A and B are shown in Fig. 16 and their frequency responses are shown in Fig. 17. The filters have enough acceptance to the tune shift. However, in these figures,

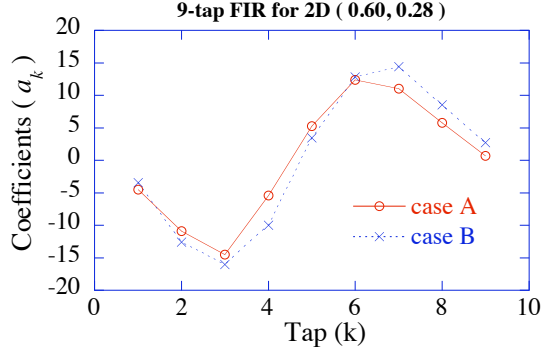


FIG. 16: Coefficients of the 9-tap FIR filters for the single-loop two-dimensional transverse feedback for cases A and B.

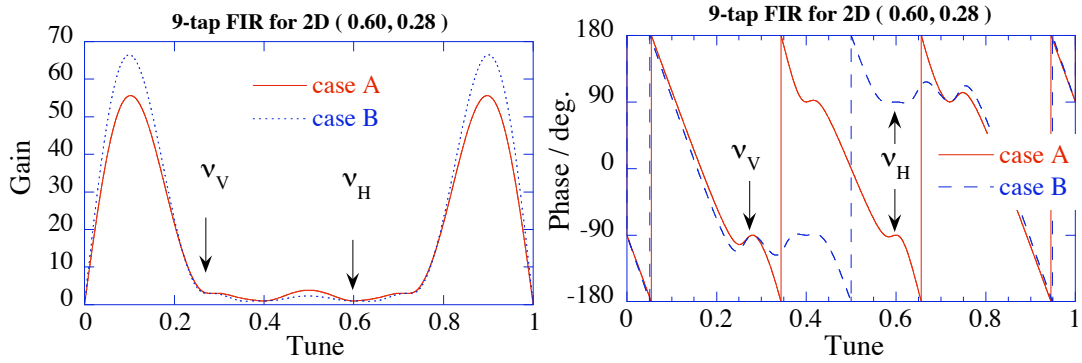


FIG. 17: Frequency responses of the gain and phase of the 9-tap FIR filters shown in Fig. 16, for single-loop two-dimensional transverse feedback for case A (solid line) and B (dotted line). The gain is normalized by the gain at the horizontal tune ($\Delta\nu = 0.60$).

we can see that the gain at tunes other than the target tunes of 0.60 and 0.28 is nearly two orders of magnitude higher than the gain at the target tunes. This raises the possibility of the saturation of the system by noise or the beam position signal produced by a synchrotron motion if the BPM is at a dispersive section. Moreover, if the BPM and the kicker both are placed at dispersive sections, the feedback may drive a longitudinal oscillation as we shall discuss in Appendix IX B. If we take the every other turn data ($k = 1, 3, 5, \dots, 17$) to make a 9-tap FIR filter, the gain at tunes other than the target tunes is lower however the acceptance to the horizontal tune shift is too narrow for actual application as shown in Fig. 18.

To suppress such high gain at tunes other than the target tunes, we can make more tap filters with the TDLSF method. As examples, we show a 12-tap and a 17-tap FIR filters of

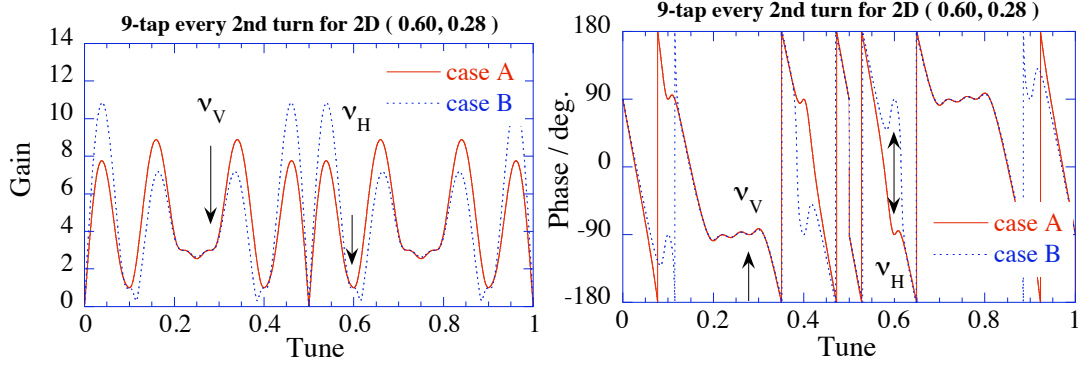


FIG. 18: Frequency responses of the gain and phase of the 9-tap FIR filters with every 2nd turn position data ($k = 1, 3, 5, 7, \dots, 17$) for case A (solid line) and B (dotted line). The gain at tunes other than target tunes are smaller than the 9-tap FIR filter with every single turn position data in Fig. 17. However the acceptance for the horizontal tune is much narrower.

which the coefficients and the frequency responses are in Fig. 19 and Fig. 20, respectively. The frequency responses of those FIR filters have narrower acceptance to the tune shift than that of 9-tap FIR filters in Fig. 17 and those acceptances are still not sufficient for the practical application to the Photon Factory ring. Thus, we used a 20-tap FIR filter for case B with the following "tuned" condition:

$$\{(\Delta\nu^{(m)}, G^{(m)}, \zeta^{(m)}, O^{(m)}) : m = 1, 2, 3, 4\} = \left\{ \left(0.58, 1, \frac{\pi}{2}, 0\right), \left(0.61, 1, \frac{\pi}{2}, 1\right), \left(0.26, 3, -\frac{\pi}{2}, 0\right), \left(0.28, 3, -\frac{\pi}{2}, 1\right) \right\} \quad (74)$$

Because the BPM are placed at a dispersive section at the ring, the contamination of low frequency position signal produced by synchrotron motion is large and we set $(G^{(0)}, O^{(0)}) = (0, 2)$ for DC to remove this low frequency signal. The minimum required number of taps N_c (Eq. (41)) for this condition is 15 and we choose 20-tap by its moderate gain at tunes other than the target tunes and moderate tune acceptance. The coefficients of the filter are shown in Fig. 21 and its frequency response is shown in Fig. 22. The gain at tunes other than target tunes are rather higher than the FIR filters shown in Fig. 20, however, the acceptance to the tune shift is much larger.

In most transverse kickers for storage rings, four skewed position stripline electrodes are employed and, if we use all of them, a feedback processor has to perform two FIR filters for cases A and B simultaneously as done by the SPring-8 feedback processor[30].

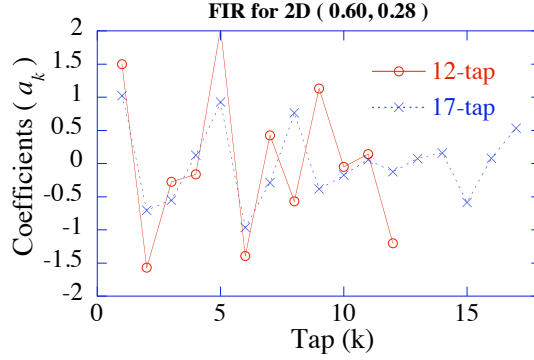


FIG. 19: Coefficients of the 12-tap and 20-tap FIR filters for the single-loop two-dimensional feedback.

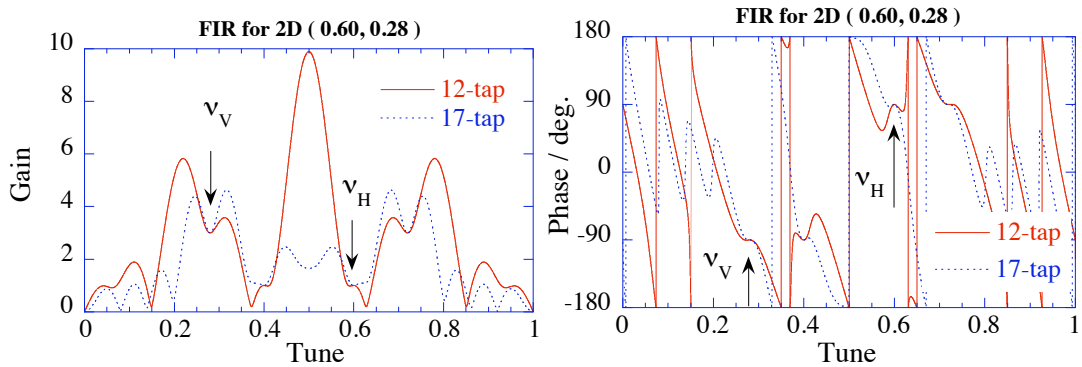


FIG. 20: Frequency responses of the gain and phase of the 12-tap and 17-tap FIR filters for two-dimensional feedback for cases B. The gain is normalized by the gain at horizontal tune ($\Delta\nu = 0.60$).

The stability of the feedback with the 9-tap and 20-tap FIR filters is summarized in Table III.

In addition, if we use an FIR filter which has zero gain at one of the transverse directions, such feedback can operate as an one-dimensional transverse feedback.

We have to note the limitations of this single-loop two-dimensional scheme. It is difficult to produce adequate FIR filters if the difference of horizontal and vertical tunes is small and the difference of the horizontal and vertical betatron phase advances between the BPM and the kicker is large [51] because the phase of such FIR filter changes so rapidly in the frequency response therefore the tune acceptance is small. And also it is difficult to apply this scheme if the difference of horizontal and vertical tunes is so small that the horizontal and vertical oscillation are coupled to produce a diagonal oscillation mode which the skewed position BPM and kicker can not detect and kick.

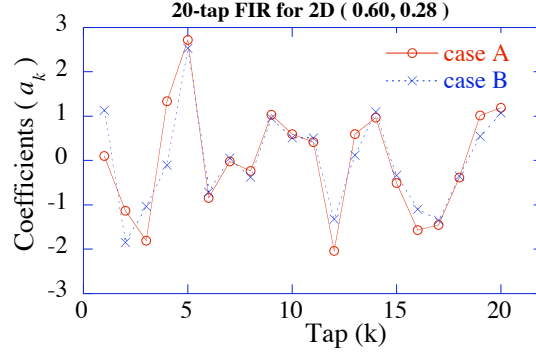


FIG. 21: Coefficients of the 20-tap FIR filters for the single-loop two-dimensional feedback.

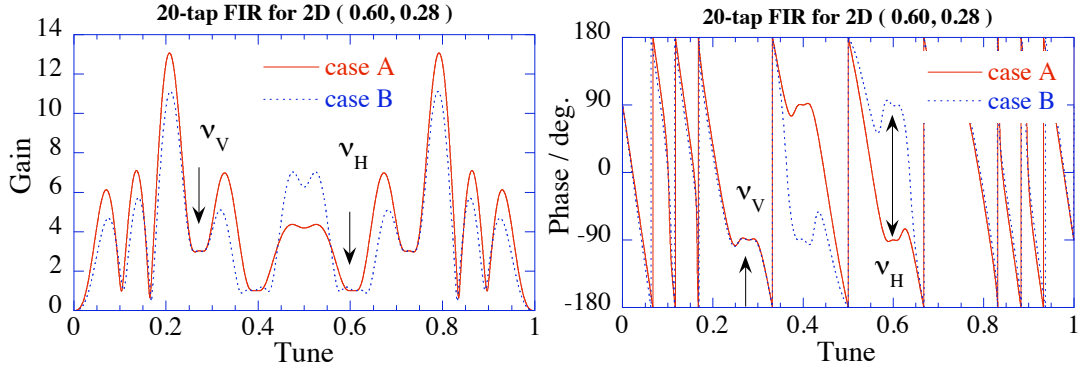


FIG. 22: Frequency responses of the gain and phase of the 20-tap FIR filters for two-dimensional feedback for cases A and B. The gain is normalized by the gain at horizontal tune ($\Delta\nu = 0.60$).

TABLE III: Stability of 9-tap and 20-tap FIR filters for two-dimensional transverse feedback. In the row for the directions, H and V indicate the horizontal and vertical directions, respectively.

configuration	9-tap				20-tap			
	A	V	H	V	A	V	H	V
direction	H	V	H	V	H	V	H	V
$\Delta\nu_0 = \phi_0/(2\pi)$	0.60	0.28	0.60	0.28	0.60	0.28	0.60	0.28
$\Delta\nu_1 = \phi_1/(2\pi)$	0.95	0.17	0.84	0.16	0.55	0.21	0.50	0.21
$\zeta(\phi_1)/\text{deg.}$	180	0	0	0	0	0	180	0
$ \tilde{G}(\Delta\nu_0)/\tilde{G}(\Delta\nu_1) $	1/42	1/13	1/47	1/16	1/3.4	1/4.0	1/6.3	1/3.7
$ T_0/\tau_{FB} $	14	18	21	21	14	8.9	19	8
simulation	14	18	21	21	14	9	19	8

V. THREE-DIMENSIONAL FEEDBACK BY A SINGLE-LOOP

We will show that the scheme described above can be extended to single-loop three-dimensional feedback that uses a transverse position and a transverse kick at dispersive sections.

Single-loop horizontal-longitudinal feedback systems already proposed by Chao et al. [47]. However, they did not show the possibility of the scheme of longitudinal feedback with a transverse feedback system of which input and output are a transverse position and kick at dispersive sections, respectively. Contrary to their result, we show that the such feedback systems can be realized with a digital signal processing scheme and show the possibility of extension to single-loop three-dimensional feedback.

We assume that a BPM is composed of a pair of skewed electrodes (Fig. 15) and is placed at a dispersive section. Then, the beam position signal from the BPM is

$$S = C_H(x_H + \eta\delta) + C_Vx_V \quad (75)$$

where x_H and x_V are the horizontal and vertical position by the betatron oscillations, respectively; and δ and η are the energy shift and the dispersion function, respectively. We assume that only the horizontal dispersion function is non-zero. A transverse kicker with skewed position stripline electrodes at a dispersive section can kick the beam horizontally, vertically, and longitudinally by changing the circumference of the ring.

If we have an FIR filter that can simultaneously control the gain and phase at three tunes (two betatron tunes and the synchrotron tune), the feedback can control the beam three-dimensionally with a single signal. We will show such an FIR filter calculated with the TDLSF method.

A. Required Condition for FIR Filters

We assume that a BPM and a kicker are placed at the same location; hence, the difference in betatron phases between the monitor and the kicker is 0, and we set the horizontal and transverse beta functions at the location to β_H and β_V , respectively. We treat the case A in Fig. 15 for the configuration of the BPM and the kicker.

To obtain damping of the horizontal and vertical betatron oscillations with the fractional tunes of $\Delta\nu_H$ and $\Delta\nu_V$, respectively, we use Eqs. (129), (131), and (133) in Appendix IX A

with setting $F = 0$ and $\tilde{K}(\Delta\nu_T) = K_T e^{-i\frac{\pi}{2}}$ where $K_T = |\tilde{K}(\Delta\nu_T)|$ and the subscript T shows that the parameter attached is for horizontal ($T = H$) or vertical ($T = V$) directions. The damping rate per turn of the betatron oscillation for the direction $T = H, V$ is

$$\frac{T_0}{\tau_T} = \frac{1}{2} \beta_T K_T. \quad (76)$$

For the damping of the synchrotron oscillation with tune $\Delta\nu = \nu_s$, we use Eqs. (152), (154), and (156) in Appendix IX B with setting $P = F = W = 0$ and $\tilde{K}(\nu_s) = K_L e^{i\frac{\pi}{2}}$ where $K_L = |\tilde{K}(\nu_s)|$, and the damping rate per turn of the synchrotron oscillation is

$$\frac{T_0}{\tau_L} = \frac{1}{2} \frac{\eta^2 \omega_s}{v \alpha} K_L. \quad (77)$$

where η , ω_s , v and α are the dispersion function, the angular frequency of the synchrotron oscillation, the velocity of the beam, and the slip factor of the ring, respectively.

From Eq. (76) and (77), the requirements for the response of the FIR filter at the target tunes are

$$\tilde{K}(\Delta\nu_H) = 2 \frac{T_0}{\tau_H} \frac{1}{\beta_H} e^{-i\frac{\pi}{2}} = e^{-i\frac{\pi}{2}} K_H \quad (78)$$

$$\tilde{K}(\Delta\nu_V) = 2 \frac{T_0}{\tau_V} \frac{1}{\beta_V} e^{-i\frac{\pi}{2}} = \frac{\tau_H}{\tau_V} \frac{\beta_H}{\beta_V} e^{-i\frac{\pi}{2}} K_H \quad (79)$$

$$\tilde{K}(\nu_s) = 2 \frac{T_0}{\tau_L} \frac{v \alpha}{\eta^2 \omega_s} e^{i\frac{\pi}{2}} = \frac{\tau_H}{\tau_L} \frac{v \alpha}{\eta^2 \omega_s} \beta_H e^{i\frac{\pi}{2}} K_H. \quad (80)$$

B. Ratio of Dynamic Range

We will compare the dynamic ranges of the system for the horizontal and longitudinal directions. From Eqs. (116) and (136), we obtain the relation of the complex amplitudes of the transverse kick angle $\tilde{\theta}$, the horizontal betatron position oscillation \tilde{x}_H , and the synchrotron energy oscillation $\tilde{\delta}$ as

$$|\tilde{\theta}| = |K_H| |\tilde{x}_H| = |K_L \eta| |\tilde{\delta}|. \quad (81)$$

Thus, we have the ratio of the dynamic ranges as

$$\left| \frac{\tilde{\delta}}{\tilde{x}_H} \right| = \left| \frac{K_H}{K_L} \frac{1}{\eta} \right| = \left| \frac{\tau_L}{\tau_T} \frac{\eta}{\beta_T} \frac{\omega_s}{v \alpha} \right| \quad (82)$$

where we used Eqs. (76) and (77) and $|\tilde{\delta}| \simeq |(\omega_s/\alpha)\tilde{\tau}|$ that is obtained from Eqs. (138) and (139) and $\tilde{\tau}$ is the amplitude of the synchrotron timing oscillation of the bunch.

TABLE IV: Longitudinal parameters of the Photon Factory ring.

Parameters	Symbol	Value
Momentum compaction factor	α	5×10^{-3}
Dispersion	η	0.5 m
Revolution Period	T_0	624 ns
Synchrotron Tune	ν_s	0.014
Velocity of the beam	v	$c = 3.0 \times 10^8$ m/s

C. Example: Photon Factory Ring

We will discuss single-loop three-dimensional feedback with the parameters of the Photon Factory ring shown in Table II and Table IV. In this discussion, contrary to Table II, we set the ratio of the sensitivity of BPM to one ($C_H/C_V = 1$).

In most cases, the required longitudinal feedback damping time is rather longer than the transverse feedback damping time. Therefore, we assume that

$$\tau_H = \tau_V = 0.2\tau_L. \quad (83)$$

We also assume that we use the kicker stripline at position #4 in Fig. 15; then we have to flip the polarity of the FIR filter at the vertical tune.

Then, from Eqs. (78), (79), and (80), the condition for the FIR filter is

$$\{(\Delta\nu^{(m)}, G^{(m)}, \zeta^{(m)}, O^{(m)}) : m = 1, 2, 3\} = \left\{ \left(0.014, 50, \frac{\pi}{2}, O_L\right), \left(0.60, 1, -\frac{\pi}{2}, O_H\right), \left(0.28, 1, \frac{\pi}{2}, O_V\right) \right\} \quad (84)$$

where $O_{L,H,V}$ are the adequate orders of expansion.

The dynamic range ratios in Eq. (82) with the condition of Eq. (83) are

$$\left| \frac{\tilde{\delta}}{\tilde{x}_H} \right| = \left| \frac{\tilde{\delta}}{\tilde{x}_V} \right| = 4 \times 10^{-5} / \text{mm} \quad (85)$$

or

$$\left| \frac{\tilde{\tau}}{\tilde{x}_H} \right| = \left| \frac{\tilde{\tau}}{\tilde{x}_V} \right| = 1.4 \text{ ps/mm}. \quad (86)$$

These ratios are typical values of longitudinal and transverse feedback systems, and the required power for the kicker is the same as that for typical transverse feedback systems.

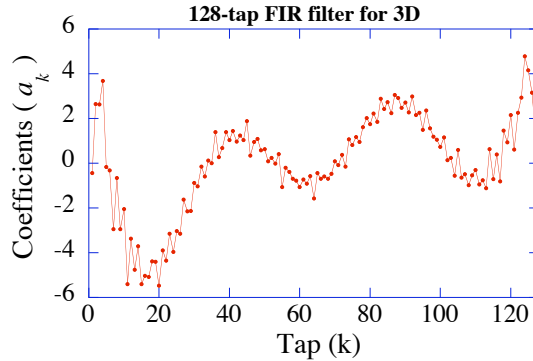


FIG. 23: Coefficients of the FIR filter for single-loop three-dimensional feedback with the tuned condition shown in Table V.

We will show a 128-tap FIR filter with a one-turn delay as an example. For the calculation of its coefficients with the TDLSF method, we use the tuned condition listed in Table V instead of the naive condition of Eq. (84) to obtain wider tune acceptance.

TABLE V: Tuned condition for the TDLSF method to obtain the 128-tap FIR filter for single-loop three-dimensional feedback

$\Delta\nu^{(m)}$	$G^{(m)}$	$\zeta^{(m)}$	$O^{(m)}$	$\Delta\nu^{(m)}$	$G^{(m)}$	$\zeta^{(m)}$	$O^{(m)}$
0.014	50	$\frac{\pi}{2}$	2	0.56	1	$-\frac{\pi}{2}$	1
0.24	1	$\frac{\pi}{2}$	1	0.57	1	$-\frac{\pi}{2}$	0
0.25	1	$\frac{\pi}{2}$	0	0.58	1	$-\frac{\pi}{2}$	1
0.26	1	$\frac{\pi}{2}$	1	0.59	1	$-\frac{\pi}{2}$	0
0.27	1	$\frac{\pi}{2}$	0	0.60	1	$-\frac{\pi}{2}$	2
0.28	1	$\frac{\pi}{2}$	2	0.61	1	$-\frac{\pi}{2}$	0
0.29	1	$\frac{\pi}{2}$	0	0.62	1	$-\frac{\pi}{2}$	1
0.30	1	$\frac{\pi}{2}$	1	0.63	1	$-\frac{\pi}{2}$	0
0.31	1	$\frac{\pi}{2}$	0	0.64	1	$-\frac{\pi}{2}$	1
0.32	1	$\frac{\pi}{2}$	1				

The coefficients of the 128-tap FIR filter are shown in Fig. 23, and its frequency response is shown in Fig. 24 and Fig. 25.

Following the analysis on the stability of the feedback in Appendix IX C, we obtained

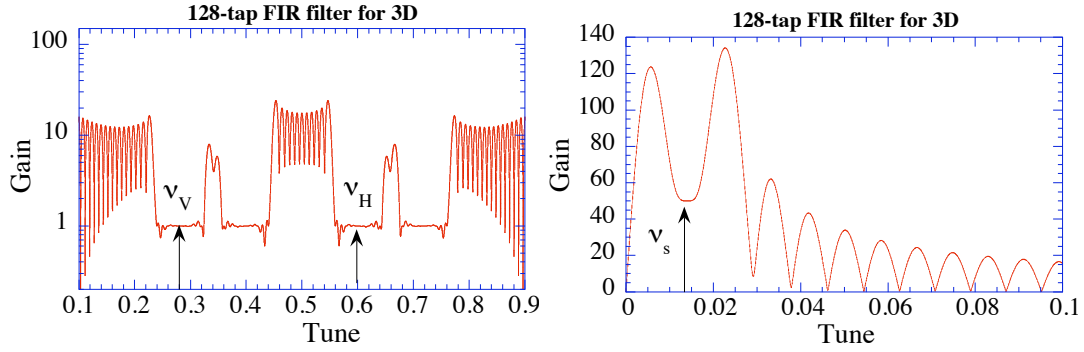


FIG. 24: Frequency response of the gain of the 128-tap FIR filter for three-dimensional feedback shown in Fig. 23. The betatron and synchrotron tunes are indicated by the arrows. The gain is normalized by the gain at horizontal and vertical target tunes ($\Delta\nu = 0.60, 0.28$).

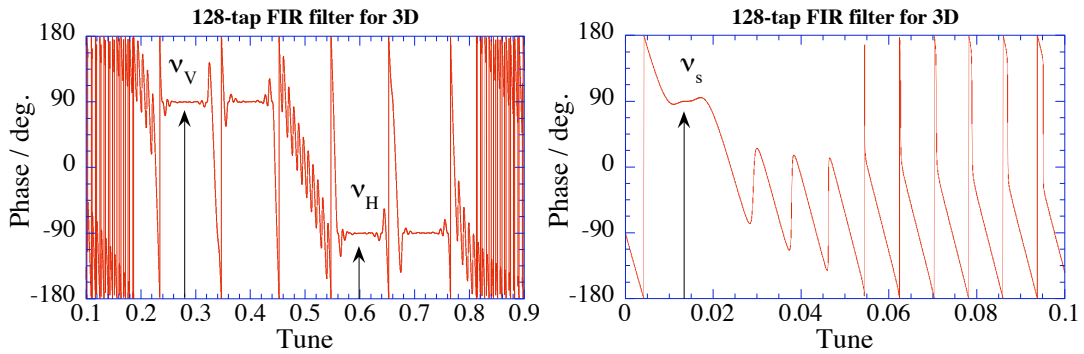


FIG. 25: Frequency response of the phase of the 128-tap FIR filter for three-dimensional feedback shown in Fig. 23. The betatron and synchrotron tunes are indicated by arrows.

the maximum stable feedback damping rates for three directions and those are shown in Table VI. The gain of the 128-tap FIR filter in the vicinity of the synchrotron tune is much larger than the gain at the betatron tunes and this high gain drives vertical betatron oscillations unstable in the vicinity of the synchrotron tune as seen in the simulation result in Fig. 26.

In addition, if we can set the gain at the horizontal and/or vertical tune to zero, we can use this as one-dimensional longitudinal feedback as previously discussed in Section III C, or as two-dimensional horizontal-longitudinal or two-dimensional vertical-longitudinal feedback.

TABLE VI: Transverse and longitudinal stability of 128-tap FIR filters for three-dimensional feedback. The polarity of the feedback is inverted for vertical and the required phase at $\Delta\nu_1$ for the tune shift from $\Delta\nu_0$ is also inverted.

Direction	Horizontal	Vertical	Longitudinal
$\Delta\nu_0$	0.60	0.28	0.014
$\Delta\nu_1$	0.50	0.0042	0.0042
$\zeta_1/\text{deg.}$	0	180	180
$ \tilde{G}(\Delta\nu_0)/\tilde{G}(\Delta\nu_1) $	1/18	1/114	1/2.3
$ T_0/\tau_{FB} $	1/54	1/94	1/57
simulation	1/54	1/94	1/57

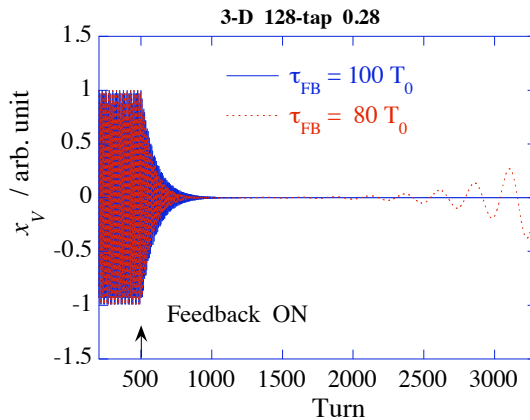


FIG. 26: The simulation result with Eq. (119) for the vertical betatron oscillation of $\Delta\nu_0 = 0.28$ with two horizontal damping times: $100T_0$ (solid line) and $80T_0$ (dotted line). The 128-tap FIR filter shown in Fig. 23 is used for the simulation. With the damping time $80T_0$, the beam is unstable at $\Delta\nu = 0.004$ where the phase shift is 180 deg., as seen in Fig. 25.

D. Comparison of Transverse Kicker and Energy Kicker

In this scheme, we use a transverse kicker to control the longitudinal motion. On the other hand, energy kickers are widely used for longitudinal feedback. We will calculate the required drive power for both cases.

From Eqs. (136) and (137), we obtain the required kick amplitudes for transverse kicker

$\tilde{\theta}$ and for energy kickers \tilde{U} as

$$\tilde{\theta} = \tilde{K}\eta\tilde{\delta} \quad (87)$$

$$\frac{\tilde{U}}{E_0} = \tilde{P}\tilde{\tau}. \quad (88)$$

If we set the phase of \tilde{K} and \tilde{P} for maximum damping as $\tilde{K} = iK_I$ and $\tilde{P} = iP_I$, then, from Eq. (152), we obtain

$$\tilde{K} = i\frac{2v}{\eta^2}\frac{\alpha}{\omega_s}\phi_I \quad (89)$$

for the transverse kicker and

$$\tilde{P} = i\frac{2\omega_s}{\alpha}\phi_I \quad (90)$$

for the energy kicker. Inserting these into Eqs. (87) and (88) yields the required amplitude of the transverse and energy kick for damping rate ϕ_I and dynamic range $\tilde{\tau}$ or $\tilde{\delta}$ as

$$\tilde{\theta} = i\frac{2v}{\eta}\frac{\alpha}{\omega_s}\phi_I\tilde{\delta} \simeq \frac{2v}{\eta}\phi_I\tilde{\tau} \quad (91)$$

$$\frac{\tilde{U}}{E_0} = i\frac{2\omega_s}{\alpha}\phi_I\tilde{\tau} \simeq -2\phi_I\tilde{\delta} \quad (92)$$

where we use $\frac{\omega_s}{\alpha}\tilde{\tau} \simeq i\tilde{\delta}$ obtained from Eqs. (138) and (139).

Table VII lists the power required for several types of feedback kickers: a horizontal-vertical kicker with four skewed positioned striplines; a horizontal dedicated kicker with two striplines; and an energy kicker. The parameters of the kickers are listed in Table II and Table IV remembering that we set the ratio of the sensitivity of the BPM to horizontal and vertical directions to one ($C_H/C_V = 1$). The transverse kicker length is assumed to be 0.3m long. The shunt impedance of the energy kicker is typical value for rings with RF frequency $\sim 500\text{MHz}$ [31, 33, 52, 53]. The shunt impedances of the transverse kicker are scaled from those of the skewed positioned stripline kicker installed in the SPring-8 ring and from the dedicated horizontal kicker designed for the SPring-8 ring. Kickers dedicated to horizontal direction usually have more impedance [54], however, the vertical betatron motion should be controlled by another loop if necessary.

The result shows that feedback with the transverse kickers requires more power than with the energy kicker; however, such power levels are commonly used in transverse feedback systems.

TABLE VII: Comparison of the required power of transverse kickers and an energy kicker (longitudinal kicker) for the timing dynamic range of $|\tilde{\tau}| = 1$ ps and the longitudinal damping time $\tau_{FB} = 1$ ms ($\phi_I = 6.24 \times 10^{-4}$) with the parameters of the Photon Factory ring listed in Table II and Table IV. The shunt impedance is defined as $R_{sh} = \frac{V^2}{2P}$ where V and P are kick voltage and power, respectively.

kick direction	horizontal and vertical	horizontal	energy
kick	$ \tilde{\theta} = 7.5 \times 10^{-7}$	rad	$ \tilde{U} /E_0 = 3.5 \times 10^{-8}$
Voltage	1900 V		88 V
kicker type	four skewed striplines	two striplines	cavity
Shunt impedance	5.3 k Ω	25 k Ω	500 Ω
Power/stripline	75 W / stripline	35 W / stripline	7.7 W

VI. SUMMARY

We proposed single-loop two-dimensional feedback systems with the FIR filters that can control the phase and gain at multiple frequencies/tunes and such systems are successfully operating at several rings. We also proposed a scheme of longitudinal feedback by a transverse feedback at a dispersive section, and with this scheme, we discussed the possibility of the single-loop three-dimensional feedback that controls two-dimensional betatron oscillation and synchrotron oscillation, simultaneously. In this scheme, the setup is the same as in the transverse feedback system, and no energy kickers are necessary.

We demonstrate a time domain least square fitting method to obtain the coefficients of finite impulse response filters for feedback. With this method we can make longer tap filters without additional constraints and with such filters we can reduce the gain at tunes other than target tunes to reduce noise to kickers to avoid the saturations of power amplifiers. Also we analyzed the stability of the feedback with FIR filters is analyzed and the scheme to obtain the shortest stable damping time of the feedback

ACKNOWLEDGMENTS

The author acknowledges K. Kobayashi for help in the development of feedback systems, and is grateful to K. Soutome, M. Takao and J. Shimizu for fruitful discussions. The con-

TABLE VIII: Phase advance from a BPM to a kicker and the required parameters in Eqs. (20) and (40) for the calculation of an FIR filter. ξ_+ and ξ_- are the phase advances from the BPM to the kicker counted with the directions shown in Fig. 27. ζ_0 is the required phase shift between the beam position and kick at the kicker. The delay is n -turns.

configuration	phase advance from	required phase parameters	
	BPM to kicker	φ	ζ
M-S-K-S	$(1 + \Delta)(n\phi + \varphi)$	φ	ζ_0
M-S-K-O	$(n + 1)(1 + \Delta)\phi - \xi_-$	0	$-\xi_- + \zeta_0$
M-O-K-S	$n(1 + \Delta)\phi + \xi_+$	0	$\xi_+ + \zeta_0$

tinual encouragement and support by K. Kumagai and H. Ohkuma are highly appreciated.

The single-loop two-dimensional feedback systems were realized in the collaboration with the staff of Photon Factory, Taiwan Light Source and SOLEIL with the help of Tokyo Electron Device Ltd. for the development of the high-performance feedback processors, which are indispensable for the single-loop multi-dimensional feedback systems. The author also acknowledges to the staff of NSRL/USTC, SSRF and APS for the discussion on the application of feedback.

VII. LOCATION OF SOURCES OF TUNE SHIFT

Storage rings usually have several sources of tune shift, such as quadrupole magnets or wigglers for betatron oscillations. If the tune shift is produced by a change in the strength of regular quadrupole magnets, the sources are distributed uniformly around a ring. On the other hand, if a source is a strong wiggler without global compensation of its tune shift, the source is localized in a ring. We have to choose proper phase parameters $\varphi^{(m)}$ and $\zeta^{(m)}$ in Eqs. (20) and (40) for better compensation of the tune shift with these sources.

We will show the case of three configurations of the sources shown in Fig. 27; [M-S-K-S] : Sources are uniformly distributed around the ring, [M-S-K-O] : Sources are localized from the BPM to the kicker, and [M-O-K-S] : Sources are localized from the kicker to the BPM. The proper choice of parameters for them are listed in Table VIII.

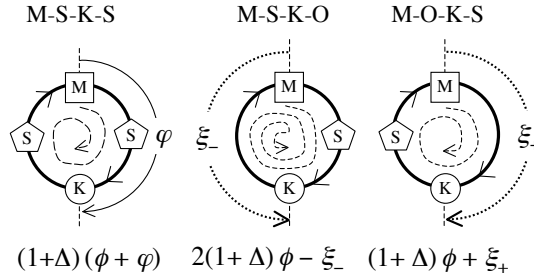


FIG. 27: Configurations of the sources of tune shift. Each circle shows a storage ring with a beam circulating clockwise. The elements flagged with M, K and S are BPMs, kickers and sets of sources of the tune shift, respectively. We show three configurations- [M-S-K-S]: sources are distributed uniformly around the ring, [M-S-K-O]: sources are localized from the BPM to the kicker, and [M-O-K-S]: sources are localized from the kicker to the BPM. The phase advances from the BPM to the kicker for the case with one-turn delay are shown below the pictures for the configurations. Dashed lines show the paths to count the phase advance from the BPM to the kicker and ξ_+ and ξ_- are the phase advances from the BPM to the kicker counted with the directions shown in the figure.

VIII. COMPARISON OF THE TDLSF METHOD WITH FREQUENCY DOMAIN APPROACH

We will illustrate a frequency domain approach for the calculation of the coefficients of FIR filters and show that the FIR filters by the TDLSF method with a special number of taps are the same as FIR filters obtained by this frequency domain approach.

We assume that the beam position has the form of Eq. (17) with $\varphi^{(m)} = 0$ and we define a vector $\phi^{(m)}$ as

$$\phi^{(m)} = \left(\phi_0^{(m)}, \phi_{-1}^{(m)}, \phi_{-2}^{(m)}, \dots, \phi_{-N}^{(m)} \right). \quad (93)$$

The response of the FIR filter for the phase advance $\phi^{(m)}$ is

$$\tilde{G}(\phi^{(m)}) = \sum_{k=0}^N a_k e^{i\phi_{-k}^{(m)}} \quad (94)$$

where a_k are the coefficients of the FIR filter and $m = 0, 1, 2, \dots, M$.

The constraints on $H(\phi^{(m)})$ to fulfill the gain and the phase at the target phase advance

$\phi^{(m)}$ is

$$\tilde{G}(\phi^{(m)}) = G^{(m)} e^{i\zeta^{(m)}} \quad (95)$$

where $G^{(m)}$ and $\zeta^{(m)}$ are the required gain and phase for the feedback. We assume that the shift of $\phi^{(m)}$ can be represented as $\Delta^{(m)}\phi^{(m)}$ and the constraint that $H(\phi^{(m)})$ remain unchanged against this small shift is

$$\tilde{G}((1 + \Delta^{(m)})\phi^{(m)}) \simeq G^{(m)} e^{i\zeta^{(m)}} \text{ for } \Delta^{(m)}\phi_k^{(m)} \ll 1. \quad (96)$$

Then, using Eq. (94), we obtain

$$\sum_{k=0}^N a_k e^{i\phi_{-k}^{(m)}} = G^{(m)} e^{i\zeta^{(m)}} \quad (97)$$

$$\sum_{k=0}^N a_k e^{i\phi_{-k}^{(m)}(1+\Delta^{(m)})} = G^{(m)} e^{i\zeta^{(m)}}. \quad (98)$$

The exponential function in the second equation can be expanded as

$$e^{i\phi_{-k}^{(m)}(1+\Delta^{(m)})} \simeq e^{i\phi_{-k}^{(m)}} (1 + i\Delta^{(m)}\phi_{-k}^{(m)}), \quad (99)$$

and we obtain

$$\sum_{k=0}^N a_k e^{i\phi_{-k}^{(m)}} = G^{(m)} e^{i\zeta^{(m)}} \quad (100)$$

$$\sum_{k=0}^N a_k \phi_{-k}^{(m)} e^{i\phi_{-k}^{(m)}} = 0, \quad (101)$$

or equivalently,

$$\sum_{k=0}^N a_k C_{-k}^{(m)} = G^{(m)} \cos \zeta^{(m)} \quad (102)$$

$$\sum_{k=0}^N a_k S_{-k}^{(m)} = G^{(m)} \sin \zeta^{(m)} \quad (103)$$

$$\sum_{k=0}^N a_k \phi_{-k}^{(m)} C_{-k}^{(m)} = 0 \quad (104)$$

$$\sum_{k=0}^N a_k \phi_{-k}^{(m)} S_{-k}^{(m)} = 0. \quad (105)$$

These are the equations for the coefficients of the FIR filter with a frequency domain approach. The number of constraints for a_k in Eqs. (102) to (105) are $4M + 2$, thus, the required number of taps of the FIR filter is $4M + 2$.

We will show that the coefficients a_k of a $4M + 2$ tap FIR filter obtained by the TDLSF method (Eq. (40)) also satisfy Eqs. (102) to (105), therefore the coefficients with the TDLSF method are the same as those with the frequency domain method. We set $\varphi^{(m)} = 0$ as in the case of the frequency domain analysis shown above. For $4M + 2$ taps, the matrix C in Eq. (28) is square and

$$D = (CC^T)^{-1}C = (C^T)^{-1}. \quad (106)$$

Then, we obtain

$$(DC^T)_{i,j} = \sum_{k=0}^N D_{i,k}C_{j,k} = \delta_{ij}. \quad (107)$$

As in the case in Eqs. (35) to (38), we assume that $P_0^{(m)}$, $Q_0^{(m)}$, $P_1^{(m)}$ and $Q_1^{(m)}$ are the j_m -th, $(j_m + 1)$ -th, $(j_m + 2)$ -th and $(j_m + 3)$ -th components of the vector \mathbf{v} . Then, from the definition of C in Eq. (28), we obtain

$$C_{j_m,k} = C_{-k}^{(m)} \quad (108)$$

$$C_{j_m+1,k} = S_{-k}^{(m)} \quad (109)$$

$$C_{j_m+2,k} = \phi_{-k}^{(m)} S_{-k}^{(m)} \quad (110)$$

$$C_{j_m+3,k} = \phi_{-k}^{(m)} C_{-k}^{(m)}. \quad (111)$$

On the other hand, from a_k in Eqs. (40) with $\varphi^{(m)} = 0$ and (107), we obtain

$$\sum_{k=0}^N a_k C_{j_m,k} = G^{(m)} \cos \zeta^{(m)} \quad (112)$$

$$\sum_{k=0}^N a_k C_{j_m+1,k} = G^{(m)} \sin \zeta^{(m)} \quad (113)$$

$$\sum_{k=0}^N a_k C_{j_m+2,k} = 0 \quad (114)$$

$$\sum_{k=0}^N a_k C_{j_m+3,k} = 0. \quad (115)$$

We apply Eqs. (108) to (111) to the L.H.S. of the above equations and we obtain the same equations as Eqs. (102) to (105). Thus, the coefficients of the $4M + 2$ -tap FIR filter

obtained with the TDLSF method fulfill the condition on the FIR filter obtained with the frequency domain approach and the coefficients of them are the same.

This frequency domain approach can produce only a $4M + 2$ tap filter for the constraint on M frequency and DC. On the other hand, the TDLSF method can produce longer tap filters of more than $4M + 2$ without additional constraints. Such longer tap filters have less gain at tunes other than target tunes and can reduce noise to avoid saturation of feedback systems.

IX. FEEDBACK SCHEME AND STABILITY

We will discuss the feedback scheme and their stability.

To simplify the discussion, we discuss the case that the phase advance of oscillation between sampling of the position data by a system is constant as $\phi_k = k\phi$ where $\phi = 2\pi\Delta\nu$ and $\Delta\nu$ is the fractional tune of the oscillation. This is typically the case for the storage ring feedback.

A. Transverse Feedback

We begin by discussing transverse feedback systems.

To control the transverse oscillation, we have several choices of the input and the output of the feedback [47]. Here, we choose the transverse position for the input and the transverse kick or the longitudinal energy kick for the output as

$$\theta_n = K \sum_{k=0}^N a_k x_{n-k} \quad (116)$$

$$\frac{U_n}{E_0} = F \sum_{k=0}^N b_k x_{n-k} \quad (117)$$

where θ_n and U_n are the transverse angle kick and the energy kick at n -th turn, respectively, and are calculated by FIR filters from transverse position data x_k , a_k and b_k are the coefficients of the FIR filters, and E_0 is the reference energy of the ring.

To simplify the discussion, we assume that the BPM and the kicker are placed at the same location. For the ring with the fractional tune of $\Delta\nu_0$, a one-turn matrix at the location of

the BPM and the kicker is

$$M_0 = \begin{pmatrix} \cos \phi_0 + \alpha \sin \phi_0 & \beta \sin \phi_0 \\ -\gamma \sin \phi_0 & \cos \phi_0 - \alpha \sin \phi_0 \end{pmatrix} \quad (118)$$

where $\phi_0 = 2\pi\Delta\nu_0$, and $\beta, \alpha = -\beta'/2$ and $\gamma = (1 + \alpha^2)/\beta$ are the Twiss parameters.

The equation of motion of the beam just downstream of the BPM and the kickers is now

$$\begin{pmatrix} x_{n+1} \\ x'_{n+1} \end{pmatrix} = M_0 \left(\begin{pmatrix} x_n \\ x'_n \end{pmatrix} + \begin{pmatrix} -\eta \frac{U_n}{E_0} \\ \theta_n - \eta' \frac{U_n}{E_0} \end{pmatrix} \right) = M_0 \left(\begin{pmatrix} x_n \\ x'_n \end{pmatrix} + \begin{pmatrix} -\eta F \sum_{k=0}^N b_k x_{n-k} \\ \sum_{k=0}^N (K a_k - \eta' F b_k) x_{n-k} \end{pmatrix} \right) \quad (119)$$

where x'_n is the angle of the beam at the n -th turn and η and η' are the dispersion function and its angle, respectively.

We assume that x_n and x'_n can be represented as

$$\begin{pmatrix} x_n \\ x'_n \end{pmatrix} = \begin{pmatrix} \tilde{x} \\ \tilde{x}' \end{pmatrix} \lambda^n. \quad (120)$$

Inserting this into Eq. (119), we obtain an eigenvalue equation for λ as

$$\lambda^2 - \left(2 \cos \phi_0 - (\cos \phi_0 + \alpha \sin \phi_0) \eta \tilde{F} + \beta \sin \phi_0 \tilde{K} \right) \lambda + 1 - \eta \tilde{F} = 0 \quad (121)$$

where we define

$$\tilde{K} = \sum_{k=0}^N (K a_k - \eta' F b_k) \lambda^{-k} \quad (122)$$

$$\tilde{F} = F \sum_{k=0}^N b_k \lambda^{-k}. \quad (123)$$

First, we will solve Eq. (121) considering that \tilde{K} and \tilde{F} are not the functions of λ but the constants.

We assume that solutions of Eq. (121) have the form of

$$\lambda_{\pm} = e^{\tilde{\kappa}} e^{\pm i(\phi_R + i\phi_I)} \quad (124)$$

where ϕ_R and ϕ_I are real values and $\tilde{\kappa}$ is a complex value. Then, we obtain

$$\lambda_+ \lambda_- \simeq 1 + 2\tilde{\kappa} \quad (125)$$

$$\lambda_+ + \lambda_- \simeq 2(1 + \tilde{\kappa}) \cos \phi_R - 2i\phi_I \sin \phi_R \quad (126)$$

where we assume that $|\tilde{\kappa}| \ll 1$ and $|\phi_I| \ll 1$.

Comparing the above equations Eqs. (125) and (126) with Eq. (121) and assuming that $|\eta\tilde{F}| \ll 1$, we obtain

$$\tilde{\kappa} = -\frac{1}{2}\eta\tilde{F} \quad (127)$$

$$\cos \phi_R = \cos \phi_0 + \frac{1}{2}(\beta K_R - \alpha\eta F_R) \sin \phi_0 \quad (128)$$

$$\phi_I \sin \phi_R = -\frac{1}{2}(\beta K_I - \alpha\eta F_I) \sin \phi_0 \quad (129)$$

where values with the subscript R or I are the real and imaginary parts, respectively, of a complex value : $A_R = \Re[\tilde{A}]$ and $A_I = \Im[\tilde{A}]$ for $\tilde{A} = A_R + iA_I$. Then, the solution of Eq. (121) is

$$\lambda = \lambda_+ = e^{\tilde{\kappa}} e^{i(\phi_R + i\phi_I)} = e^{\kappa_R - \phi_I} e^{i(\kappa_I + \phi_R)} \quad (130)$$

and the solution for λ is obtained with the values of \tilde{K} and \tilde{F} . However, \tilde{K} and \tilde{F} are the function of λ and we need to use an iteration scheme to obtain the value of λ . The total growth time τ_{tot} and the shifted phase advance per turn driven by the feedback, ϕ , are

$$\frac{T_0}{\tau_{tot}} = \frac{T_0}{\tau_I} + \kappa_R - \phi_I \quad (131)$$

$$\phi = \kappa_I + \phi_R, \quad (132)$$

where we include other growth rate of $1/\tau_I$ and T_0 is the revolution period of the ring. We assume that the growth or damping of the oscillation is small and we can approximate the functions of Eqs. (122) and (123) as

$$\tilde{K} \simeq \sum_{k=0}^N (K a_k - \eta' F b_k) e^{-ik2\pi\Delta\nu} \quad (133)$$

$$\tilde{F} \simeq F \sum_{k=0}^N b_k e^{-ik2\pi\Delta\nu}. \quad (134)$$

where we use $\Delta\nu = \frac{\phi}{2\pi}$. We represent the above functions as $\tilde{K}(\Delta\nu)$ and $\tilde{F}(\Delta\nu)$, respectively. In Appendix IX D, we will discuss the case that the growth/damping of the oscillation is large.

If the feedback is strong so enough that the tune shift produced by the feedback in Eq. (132) is sufficiently large to drive the tune ϕ to the unstable region where

$$\frac{1}{\tau_{tot}} > 0, \quad (135)$$

the beam oscillation at the shifted tune is excited by the feedback itself and the oscillation of the tune ϕ grows to the saturation of the feedback system.

B. Longitudinal Feedback

Next, we discuss longitudinal feedback systems.

We use η for the dispersion function at the BPM and the kicker, and τ and δ for the timing position of the beam and the relative energy shift, respectively.

We choose the transverse position $x = \eta\delta$ and the longitudinal timing position τ for the input to the feedback, and the transverse angle kick θ and longitudinal energy kick U for the output of the feedback as

$$\theta_n = W \sum_{k=0}^N c_k \tau_{n-k} + K \sum_{k=0}^N a_k (\eta \delta_{n-k}) \quad (136)$$

$$\frac{U_n}{E_0} = P \sum_{k=0}^N d_k \tau_{n-k} + F \sum_{k=0}^N b_k (\eta \delta_{n-k}) \quad (137)$$

where a_k, b_k, c_k and d_k are coefficients of FIR filters, and τ_n and δ_n are the longitudinal timing position and the relative energy shift at the n -th turn, respectively.

We assume that an acceleration system and the longitudinal and transverse kickers are placed at the same location. Then, the equations for the synchrotron motion just the downstream of them are

$$\tau_{n+1} = \tau_n - \alpha T_0 \delta_n - \frac{\eta}{v} \theta_n = \tau_n - \alpha T_0 \delta_n - \frac{\eta}{v} W \sum_{k=0}^N c_k \tau_{n-k} - \frac{\eta^2}{v} K \sum_{k=0}^N a_k \delta_{n-k} \quad (138)$$

$$\delta_{n+1} = \delta_n + \frac{\omega_s^2 T_0}{\alpha} \tau_{n+1} + \frac{U_{n+1}}{E_0} = \delta_n + \frac{\omega_s^2 T_0}{\alpha} \tau_{n+1} + P \sum_{k=0}^N d_k \tau_{n+1-k} + \eta F \sum_{k=0}^N b_k \delta_{n+1-k} \quad (139)$$

where α and ω_s is the dilution factor and the angular synchrotron frequency of the ring, respectively. In the above equations, we use the fact that a static transverse angle kick θ at a dispersive section produces a change in the orbit length: $\Delta C = \eta\theta$ or a change in the revolution period: $\Delta\tau = -\Delta C/v = -(\eta/v)\theta$ where v is the velocity of the beam [46]. In addition, we assume that the synchrotron frequency is so lower than the betatron frequency that the transverse kick at the synchrotron frequency is adiabatic for the betatron oscillation and we can treat such kick as static for the betatron oscillation.

We assume that we can write

$$\tau_n = \tilde{\tau} \lambda^n \quad (140)$$

$$\delta_n = \tilde{\delta} \lambda^n. \quad (141)$$

Inserting them to Eqs. (138) and (139), we obtain an eigenvalue equation for λ as

$$\lambda^2 - \left(2 - \omega_s^2 T_0^2 + \left(-\frac{\eta}{v} \tilde{W} + \eta \tilde{F} \right) - \alpha T_0 \tilde{P} - \frac{\eta^2 \omega_s^2 T_0}{\alpha v} \tilde{K} \right) \lambda + 1 - \frac{\eta}{v} \tilde{W} + \eta \tilde{F} = 0 \quad (142)$$

where

$$\tilde{K} = K \sum_{k=0}^N a_k \lambda^{-k} \quad (143)$$

$$\tilde{F} = F \sum_{k=0}^N b_k \lambda^{-k} \quad (144)$$

$$\tilde{W} = W \sum_{k=0}^N c_k \lambda^{-k} \quad (145)$$

$$\tilde{P} = P \sum_{k=0}^N d_k \lambda^{-k} \quad (146)$$

and we assume that $|\eta \tilde{F}| \ll 1$, $\frac{1}{1-\eta \tilde{F}} \simeq 1 + \eta \tilde{F}$, and the second-order terms of $\tilde{W}, \tilde{K}, \tilde{P}$ and \tilde{F} are negligibly small.

As in the discussion of transverse motion in the previous subsection, we will solve Eq. (142) considering $\tilde{K}, \tilde{W}, \tilde{P}$, and \tilde{F} as constants.

As in the transverse case, we assume that the solutions of Eq. (142) have the form of

$$\lambda_{\pm} = e^{\tilde{\kappa}} e^{\pm i(\phi_R + i\phi_I)}. \quad (147)$$

Then, we obtain

$$\lambda_+ \lambda_- \simeq 1 + 2\tilde{\kappa} \quad (148)$$

$$\lambda_+ + \lambda_- \simeq 2 \left(1 + \tilde{\kappa} - i\phi_I \phi_R - \frac{1}{2} \phi_R^2 \right) \quad (149)$$

where we assume that $|\tilde{\kappa}| \ll 1$, $|\phi_R| \ll 1$, $|\phi_I| \ll 1$ and $|\phi_I| \ll |\phi_R|$.

Comparing above equations Eqs. (148) and (149) with Eq. (142), we obtain

$$\tilde{\kappa} = \frac{1}{2} \left(-\frac{\eta}{v} \tilde{W} + \eta \tilde{F} \right) \quad (150)$$

$$\phi_R^2 = \phi_0^2 + \phi_0^2 \frac{\eta^2}{\alpha v T_0} K_R + \alpha T_0 P_R \quad (151)$$

$$\phi_I = \frac{1}{2\phi_R} \left(\phi_0^2 \frac{\eta^2}{\alpha v T_0} K_I + \alpha T_0 P_I \right) \quad (152)$$

where we set $\phi_0 = \omega_s T_0$. Thus the solution is

$$\lambda = \lambda_+ = e^{\tilde{\kappa}} e^{i(\phi_R + i\phi_I)} = e^{\kappa_R - \phi_I} e^{i(\kappa_I + \phi_R)} \quad (153)$$

where $\tilde{\kappa} = \kappa_R + i\kappa_I$ with real values of κ_R and κ_I .

Then, the solution for λ is obtained with the values of \tilde{K} , \tilde{W} , \tilde{P} , and \tilde{F} . However Those values are the function of λ and we need to use an iteration scheme to obtain the value of λ . The total damping time τ_{tot} and the shifted phase advance per turn driven by feedback, ϕ , are now

$$\frac{T_0}{\tau_{tot}} = \frac{T_0}{\tau_I} + \kappa_R - \phi_I \quad (154)$$

$$\phi = \kappa_I + \phi_R. \quad (155)$$

As in the case of transverse, we assume that the growth or damping of the oscillation is small and we can approximate the functions of Eqs. (143) to (146) as

$$\tilde{K} \simeq K \sum_{k=0}^N a_k e^{-ik2\pi\Delta\nu} \quad (156)$$

$$\tilde{F} \simeq F \sum_{k=0}^N a_k e^{-ik2\pi\Delta\nu} \quad (157)$$

$$\tilde{W} \simeq W \sum_{k=0}^N a_k e^{-ik2\pi\Delta\nu} \quad (158)$$

$$\tilde{P} \simeq P \sum_{k=0}^N a_k e^{-ik2\pi\Delta\nu} \quad (159)$$

$$(160)$$

where we use $\Delta\nu = \frac{\phi}{2\pi}$. We represent the above functions as $\tilde{K}(\Delta\nu)$, $\tilde{F}(\Delta\nu)$, $\tilde{W}(\Delta\nu)$, and $\tilde{P}(\Delta\nu)$, respectively. In Appendix IX D, we will discuss the case that the growth or damping of the oscillation is high.

As in the case of the transverse feedback, if the feedback is strong so enough that the tune shift by the feedback in Eq. (155) is sufficiently large to drive tunes ϕ to the unstable region where

$$\frac{1}{\tau_{tot}} < 0, \quad (161)$$

the beam oscillation at the shifted tune is excited by the feedback itself and the oscillation of the tune ϕ grows to the saturation of the feedback system.

C. Stability of Feedback

With the discussion above, we will discuss the stability of feedback systems to show the available shortest feedback stable damping time without the instabilities driven by the feedback itself. To simplify the discussion, we discuss the case only with feedback and without other sources of growth and the target tune and the actual tune are the same. We use $\Delta\nu_0$ for the target tune and $\Delta\nu_1$ for the tune on the boundary of the stable region of the feedback where the growth/damping is zero. We define $\phi_{0,1} = 2\pi\Delta\nu_{0,1}$.

First, we discuss the transverse feedback. We assume $F = 0$ in Eqs. (127) to (129) as in the examples shown in the main part of the study, and we set

$$\tilde{G} = \frac{1}{2}\beta\tilde{K}\sin\phi_0. \quad (162)$$

To simplify the discussion, we assume that a BPM and a kicker are placed at the same location, and the phase of a FIR filter is optimized for maximum damping rate, thus the phase of the FIR filter at the target tune $\Delta\nu_0$ is -90 deg. and the phase at the boundary, $\Delta\nu_1$, is 0 deg. or 180 deg.

Then, we obtain

$$\tilde{G}(\Delta\nu_0) = e^{-i\frac{\pi}{2}}|G_I(\Delta\nu_0)| \quad (163)$$

where G_R and G_I are the real and imaginary part of \tilde{G} , respectively. From Eqs. (128) and (129) with setting $\phi_R = \phi_1$, we obtain $\tilde{G}(\Delta\nu_1)$ required to drive the tune from $\Delta\nu_0$ to $\Delta\nu_1$ as

$$\tilde{G}(\Delta\nu_1) = G_R(\Delta\nu_1) = \frac{\cos\phi_1 - \cos\phi_0}{\sin\phi_0} \quad (164)$$

which defines the phase (0 deg. or 180 deg.) of $\tilde{G}(\Delta\nu_1)$ for ϕ_0 and ϕ_1 .

From Eq. (129), the damping rate per turn with this \tilde{G} is

$$\phi_I = -G_I(\Delta\nu_0). \quad (165)$$

From Eqs. (163) to (165), we obtain the maximum stable feedback damping rate per turn $T_0/\tau_{FB} = \phi_I$ for the transverse direction as

$$|\phi_I| = \left| \frac{\cos\phi_1 - \cos\phi_0}{\sin\phi_0} \right| \left| \frac{\tilde{G}(\Delta\nu_0)}{\tilde{G}(\Delta\nu_1)} \right|. \quad (166)$$

The value of $\left| \tilde{G}(\Delta\nu_0)/\tilde{G}(\Delta\nu_1) \right|$ can be obtained from the frequency response of the gain of the FIR filter because the gain is proportional to $|\tilde{G}(\Delta\nu)|$ as seen in Eq. (162).

For longitudinal feedback, we set $P \neq 0$, $K \neq 0$ and $W = F = 0$ in Eqs. (150) to (152), as in the examples shown in main part of the study. And we set

$$\tilde{G} = \phi_0^2 \frac{\eta^2}{\alpha\nu T_0} \tilde{K} + \alpha T_0 \tilde{P}. \quad (167)$$

We assume that the phase of a FIR filter is optimized for maximum damping rate, thus the phase of \tilde{G} at $\Delta\nu_0$ to be 90 deg. and the phase of \tilde{G} at $\Delta\nu_1$ is 0 deg. or 180 deg. Then, we obtain

$$\tilde{G}(\Delta\nu_0) = e^{i\frac{\pi}{2}} |G_I(\Delta\nu_0)|. \quad (168)$$

From Eqs. (151) to (152) with setting $\phi_R = \phi_1$, we obtain $\tilde{G}(\Delta\nu_1)$ required to drive the tune from $\Delta\nu_0$ to $\Delta\nu_1$ as

$$\tilde{G}(\Delta\nu_1) = G_R(\Delta\nu_1) = \phi_1^2 - \phi_0^2, \quad (169)$$

which defines the phase (0 deg. or 180 deg.) of $\tilde{G}(\Delta\nu_1)$ for ϕ_0 and ϕ_1 .

From Eq. (152), the damping rate per turn with this \tilde{G} is

$$\phi_I = \frac{1}{2\phi_0} G_I(\Delta\nu_0). \quad (170)$$

From Eqs. (168) to (170), the maximum stable damping rate per turn for the longitudinal direction is

$$|\phi_I| = \left| \frac{\phi_1^2 - \phi_0^2}{2\phi_0} \right| \left| \frac{\tilde{G}(\Delta\nu_0)}{\tilde{G}(\Delta\nu_1)} \right| \quad (171)$$

and $\left| \tilde{G}(\Delta\nu_0)/\tilde{G}(\Delta\nu_1) \right|$ can be obtained from the frequency response of the gain of the FIR filter because the gain is proportional to $|\tilde{G}(\Delta\nu)|$ as seen in Eq. (167).

Usually FIR filters have several candidates of unstable tunes $\Delta\nu_1$ which are on the boundaries of stable regions and satisfy the relation of the FIR filter phase and the tune shift direction shown by Eq. (164) and Eq. (169). In those tunes for $\Delta\nu_1$, the maximum stable damping rate is limited by the tune which have lowest $|\phi_I(\Delta\nu_0)|$ in Eq. (166) for transverse, and Eq. (171) for longitudinal.

D. Response of FIR filter for Growing/Damping Oscillation

Here, we will analyze the response of the FIR filters for the input of growing/damping oscillations. We assume that the input and output of the filter at the n -th turn, x_n and y_n , respectively, are growing/damping oscillations of

$$x_n = \tilde{x}e^{in(\phi+i\alpha)} \quad (172)$$

$$y_n = \tilde{y}e^{in(\phi+i\alpha)}. \quad (173)$$

where α is a growing rate per turn, $\phi = 2\pi\Delta\nu$ is the phase advance with fractional tune $\Delta\nu$, and we take their real part as a physical quantities of them. Then, the response of the FIR filter in Eq. (1) is

$$\tilde{y} = \tilde{G}(\phi + i\alpha)\tilde{x} \quad (174)$$

$$\tilde{G}(\phi + i\alpha) = \sum_{k=0}^N a_k e^{-i(\phi+i\alpha)k}. \quad (175)$$

Expanding $\tilde{G}(\phi + i\alpha)$ with α , we obtain

$$\tilde{G}(\phi + i\alpha) = \tilde{G}(\phi) + i\alpha \frac{\partial \tilde{G}(\phi)}{\partial \phi} - \frac{1}{2}\alpha^2 \frac{\partial^2 \tilde{G}(\phi)}{\partial \phi^2} + \dots \quad (176)$$

For the FIR filters for the target phase advance ϕ_0 obtained with the TDLSF method, we obtain

$$\left. \frac{\partial^r \tilde{G}(\phi)}{\partial \phi^r} \right|_{\phi=\phi_0} = 0 \quad (177)$$

where r is the order of the expansion with the shift of the phase advance $\Delta\phi$ as indicated by $O^{(m)}$ in Eq. (53). For FIR filters with $r \neq 0$, we have $\tilde{G}(\phi + i\alpha) \sim \tilde{G}(\phi)$ for small α , and the frequency response for growing/damping oscillations are the same as that for static oscillations.

We will discuss the case of

$$\left. \frac{\partial \tilde{G}(\phi)}{\partial \phi} \right|_{\phi=\phi_0} \neq 0. \quad (178)$$

We set

$$\tilde{G}(\phi) = G(\phi)e^{i\zeta(\phi)} \quad (179)$$

where $G(\phi) = |\tilde{G}(\phi)|$ and $\zeta(\phi) = \arg(\tilde{G}(\phi))$ and we obtain

$$\frac{\partial \tilde{G}(\phi)}{\partial \phi} = \left(\frac{\partial G(\phi)}{\partial \phi} \frac{1}{G(\phi)} + i \frac{\partial \zeta(\phi)}{\partial \phi} \right) \tilde{G}(\phi). \quad (180)$$

If $\alpha \ll 1$, we take the first order of α in Eq. (176) and obtain

$$\tilde{G}(\phi + i\alpha) = \tilde{G}(\phi) \left(1 - \alpha \frac{\partial \zeta(\phi)}{\partial \phi} + i\alpha \frac{\partial G(\phi)}{\partial \phi} \frac{1}{G(\phi)} \right), \quad (181)$$

and, with the approximation:

$$1 - \alpha \frac{\partial \zeta(\phi)}{\partial \phi} + i\alpha \frac{\partial G(\phi)}{\partial \phi} \frac{1}{G(\phi)} \sim e^{-\alpha \frac{\partial \zeta(\phi)}{\partial \phi}} e^{i\alpha \frac{\partial G(\phi)}{\partial \phi} \frac{1}{G(\phi)}}, \quad (182)$$

we obtain

$$\tilde{G}(\phi + i\alpha) = \tilde{G}(\phi) e^{\alpha \frac{\partial \zeta(\phi)}{\partial \phi}} e^{i\alpha \frac{\partial G(\phi)}{\partial \phi} \frac{1}{G(\phi)}}. \quad (183)$$

Then, from Eqs. (172) to (175), we obtain

$$\tilde{y} e^{-\alpha n} e^{in\phi} = \tilde{G}(\phi) \tilde{x} e^{-\alpha(n - \frac{\partial \zeta(\phi)}{\partial \phi})} e^{i(n\phi + \alpha \frac{\partial G(\phi)}{\partial \phi} \frac{1}{G(\phi)})}. \quad (184)$$

This form shows that the amplitude growth of y_n has a delay $\frac{\partial \zeta}{\partial \phi}$ compared with the amplitude growth of x_n , and y_n has a phase shift $\alpha \frac{\partial G}{\partial \phi} \frac{1}{G}$ compared with x_n . This amplitude delay is the group delay of the FIR filter as expected by its definition for FIR filters. In addition, the phase shift produced by $\alpha \frac{\partial G}{\partial \phi} \frac{1}{G}$ for growing/damping oscillation reduce the area of stable region. We need to consider these effects if such FIR filters are used for feedback.

We will show two examples of transverse feedback with 9-tap FIR filters with 5-turn delay: the input position data of $k = -5, -6, -7, -8, -9, -10, -11, -12, -13$ and the target tune 0.15 ($\phi_0 = 0.94$). First example is a FIR filter with 0th order expansion ($r = 0$ and $\frac{\partial \zeta}{\partial \phi}|_{\phi=\phi_0} = 8.5$ in Eq. (177)) with the condition for the TDLSF method:

$$(\Delta\nu, G, \zeta, O) = \left(0.15, 1, -\frac{\pi}{2}, 0 \right) \quad (185)$$

and this is the simple band-pass filter. The second is the FIR filter with first order expansion ($r = 1$ and $\frac{\partial \zeta}{\partial \phi}|_{\phi=\phi_0} = 0$) with the condition:

$$(\Delta\nu, G, \zeta, O) = \left(0.15, 1, -\frac{\pi}{2}, 1 \right). \quad (186)$$

For both cases, we set $(G^{(0)}, O^{(0)}) = (0, 0)$ for DC.

Their frequency responses are shown in Fig. 28. For the FIR filter with $\frac{\partial\zeta}{\partial\phi} = 8.5$, the variation of the phase to the tune shift is much larger, thus the tune acceptance is narrower than those of the FIR filter with $\frac{\partial\zeta}{\partial\phi} = 0$. Using Eq. (119) with setting $F = 0$, we simulated a feedback with a feedback damping rate $1/(15T_0)$ for the growing oscillation with a growth rate $1/(20T_0)$. The results are shown in Fig. 29 where the feedback is turned on at the 500th turn.

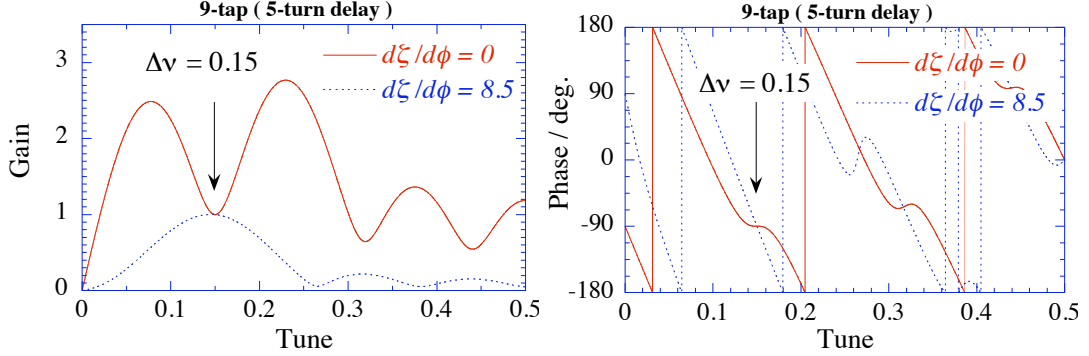


FIG. 28: Frequency response of the 5-turn delay 9-tap FIR filters with $\frac{\partial\zeta}{\partial\phi} = 0$ (solid line) and with $\frac{\partial\zeta}{\partial\phi} = 8.5$ (dotted line). The target tune is 0.15 which is shown by arrows.

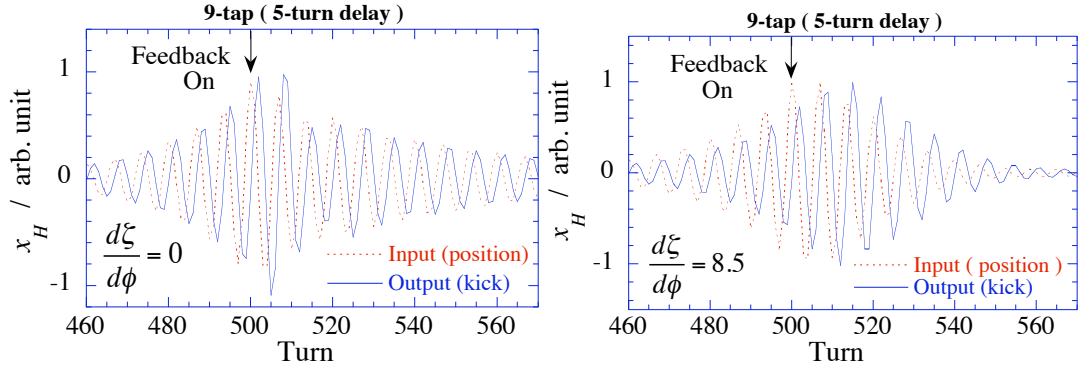


FIG. 29: Simulation result for the response of the 5-turn delay 9-tap FIR filters with $\frac{\partial\zeta}{\partial\phi} = 0$ and $\frac{\partial\zeta}{\partial\phi} = 8.5$ for the oscillation with the growing rate $1/(20T_0)$ with the feedback damping rate $1/(15T_0)$. The feedback is turned on at 500th turn. The input (position) and the output (kick) of the FIR filters are shown by dotted and solid lines, respectively.

For the growing part of the oscillation before the 500th turn in Fig. 29, we can observe a delay in the growth of the amplitude, $8.4T_0$, for the FIR filter with $\frac{\partial\zeta}{\partial\phi} = 8.5$ which is close to the expected value. The delay is $1.1T_0$ for the FIR filter with $\frac{\partial\zeta}{\partial\phi} = 0$ and is well

compensated compared with the FIR filter with $\frac{\partial\zeta}{\partial\phi} = 8.5$.

For both FIR filters, the simulations show that the maximum stable damping rate with those filters are limited by the phase shift to an unstable region produced by the feedback itself, and are $1/(8.0T_0)$ at the shifted tune $\Delta\nu_1 = 0.096$ for the FIR filter with $\frac{\partial\zeta}{\partial\phi} = 0$ and $1/(3.1T_0)$ at the shifted tune $\Delta\nu_1 = 0.10$ for the FIR filter with $\frac{\partial\zeta}{\partial\phi} = 8.5$. These values agree well with those calculated in Eq. (166). This result shows that the effect of group delay on such a stability limit is small as expected.

For the damping part of the oscillation in Fig. 29, we can observe an increase of the damping rate with the FIR filter with $\frac{\partial\zeta}{\partial\phi} = 8.5$ compared with that with the filter with $\frac{\partial\zeta}{\partial\phi} = 0$. The reason of this change of the gain is that the FIR filter with group delay produces more output than a FIR filter without group delay for the damping oscillation. For a growing oscillation, such group delay reduces the feedback damping effect. However, the necessary feedback gain to overcome the growth of the oscillation is the same in these two FIR filters because the feedback damping reduces the total growth rate and the effect of the group delay become smaller.

-
- [1] T. Nakamura, K. Kobayashi, and T. Ohshima, in *Proceedings of 1st Annual Meeting of Particle Acc. Soc. of Japan* (2004), p. 619, URL http://www.pasj.jp/web_publish/pasj1_lam29/proceedings.html.
 - [2] T. Ohshima, H. Tanaka, K. Soutome, S. Matsui, M. Takao, M. Masaki, H. Ohkuma, and N. Kumagai, in *Proceedings of EPAC 2004* (2004), p. 414.
 - [3] L. Merminga, D. R. Douglas, and G. A. Krafft, in *Proceedings of LINAC 2002* (2002), p. 600.
 - [4] T. Kasuga, M. Hasumoto, T. Kinoshita, and H. Yonehara, *Jpn. J. Appl. Phys.* **27**, 100 (1988).
 - [5] H. Hindi, N. Eisen, J. Fox, I. Linscott, G. Oxoby, and L. Sapozhnikov, in *Proceedings of PAC 1993* (1993), p. 2352.
 - [6] G. Stover, J. Fox, D. Teytelman, and A. Young, in *Proceedings of PAC 1999* (1999), p. 1213.
 - [7] M. Tobiyama and E. Kikutani, in *Proceedings of PAC 1997* (1997), p. 2335.
 - [8] K. Balewski, in *Proceedings of EPAC 1998* (1998), p. 169.
 - [9] W. Barry, J. Corlett, M. Fahmie, J. Greer, G. Lambertson, and C. Pike, in *Proceedings of PAC 1997* (1997), p. 2344.

- [10] D. Teytelman, R. Claus, J. Fox, H. Hindi, I. Linscott, S. Prabhakar, W. Ross, A. Young, A. Drago, and M. Serio, in *Proceedings of ICALEPCS 1999* (1999), p. 252.
- [11] J. Fox, S. Prabhakar, D. Teytelman, A. Young, G. Stover, A. Drago, M. Serio, S. Khan, T. Knuth, Y. J. Kim, et al., in *SLAC-BUB-8410 / Proceedings of BIW2000* (2000).
- [12] M. Tobiyama and E. Kikutani, *Phys. Rev. ST Accl. Beams* **3**, 012801 (2000).
- [13] M. Tobiyama, E. Kikutani, J. Flanagan, and S. Hiramatsu, in *Proceedings of PAC 2001* (2001), p. 1246.
- [14] A. Drago, C. Biscari, A. Gallo, A. Ghigo, F. Marcellini, C. Milardi, M. Serio, A. Stella, M. Zobov, J. Fox, et al., in *Proceedings of PAC 2001* (2001), p. 3543.
- [15] A. Drago, A. Argan, and M. Serio, in *Proceedings of ICALEPCS 2001* (2001), p. 376.
- [16] H. S. Kang, W. H. Hwang, H. J. Park, D. T. Kim, J. Huang, and S. H. Nam, in *Proceedings of APAC 2001* (2001), p. 311.
- [17] H. S. Kang, W. H. Hwang, H. J. Park, D. T. Kim, Y. J. Han, J. Huang, and S. H. Nam, in *Proceedings of EPAC 2002* (2002), p. 2076.
- [18] D. Teytelman, in *Proceedings of PAC 2003* (2003), p. 318.
- [19] D. Bulfone, C. J. Bocchetta, R. Bressanutti, A. Carniel, G. Causero, A. Fabris, A. Gambitta, D. Giuressi, G. Loda, M. Lonza, et al., in *Proceedings of DIPAC 2001* (2001), p. 66.
- [20] D. Bulfone, V. Forchi', M. Lonza, L. Zambon, and M. Dehler, in *Proceedings of EPAC 2002* (2002), p. 2061.
- [21] D. Bulfone, V. Forchi', M. Lonza, L. Zambon, and M. Dehler, in *Proceedings of PAC 2003* (2003), p. 3395.
- [22] D. Bulfone, V. Forchi', M. Lonza, L. Zambon, and M. Dehler, in *Proceedings of ICALEPCS 2003* (2003), p. 32.
- [23] S. Khan and T. Knuth, in *Proceedings of PAC 2001* (2001), p. 1871.
- [24] M. Dehler, R. Kramert, P. Pollet, T. Schilcher, D. Bulfone, and M. Lonza, in *Proceedings of EPAC 2004* (2004), p. 2508.
- [25] M. Dehler, G. Marinkovic, R. Kramert, P. Pollet, and T. Schilcher, in *Proceedings of APAC 2007* (2007), p. 118.
- [26] E. Plouviez, P. Arnoux, F. Epaud, J. Jacob, J. M. Koch, N. Michel, G. Naylor, J.-L. Revol, V. Serriere, and D. Vial, in *Proceedings of EPAC 2006* (2006), p. 2976.
- [27] D. Teytelman, C. Rivetta, D. V. Winkle, R. Akre, J. Fox, A. Krasnykh, A. Drago, J. Flanagan,

- T. Naito, and M. Tobiyama, in *Proceedings of EPAC 2006* (2006), p. 3038.
- [28] T. Nakamura, S. Date, K. Kobayashi, and T. Ohshima, in *Proceedings of EPAC 2004* (2004), p. 2649.
- [29] T. Nakamura and K. Kobayashi, in *Proceedings of ICALEPCS 2005* (2005), P3 022.
- [30] T. Nakamura, K. Kobayashi, W. Cheng, T. Honda, M. Izawa, T. Obina, and M. Tadano, in *Proceedings of EPAC 2006* (2006), p. 3006.
- [31] W. Cheng, T. Obina, T. Honda, M. Izawa, M. Tadano, M. Tobiyama, T. Nakamura, and K. Kobayashi, in *Proceedings of EPAC 2006* (2006), p. 3009.
- [32] W. Cheng and T. Obina, in *Proceedings of APAC 2007* (2007), p. 330.
- [33] C. Kuo, W. Lau, M. Yeh, K. Hu, D. Lee, M. Wang, P. Chou, D. Lee, S. Hsu, J. Chen, et al., in *Proceedings of EPAC 2006* (2006), p. 3023.
- [34] K. H. Hu, C. H. Kuo, P. J. Chou, D. Lee, S. Y. Hsu, J. Chen, C. J. Wang, K. T. Hsu, K. Kobayashi, T. Nakamura, et al., in *Proceedings of EPAC 2006* (2006), p. 3020.
- [35] C. H. Kuo, K. H. Hu, D. Lee, J. Chen, S. Y. Hsu, and K. T. Hsu, in *Proceedings of APAC 2007* (2007), p. 419.
- [36] K. H. Hu, D. Lee, S. Y. Hsu, P. C. Chiu, C. H. Kuo, J. Chen, and K. T. Hsu, in *Proceedings of PAC 2007* (2007), p. 383.
- [37] R. Nagaoka, L. Cassinari, J. C. Denard, J. M. Filhol, N. Hubert, M. P. Level, P. Marchand, C. Mariette, F. Ribeiro, R. Sreedharan, et al., in *Proceedings of PAC 2007* (2007), p. 161.
- [38] Z. Zhou, J. Wang, B. Sun, L. Huang, K. Zheng, Y. Yang, Y. Chen, T. Nakamura, and K. Kobayashi, in *Proceedings of PAC 2007* (2007), p. 278.
- [39] V. Cherepanov, E. Dementev, A. Medvedko, V. Smaluk, and D. Sukhanov, in *Proceedings of RuPAC 2006* (2006), p. 238.
- [40] C.-Y. Yao, E. Norum, and N. DiMonte, in *Proceedings of PAC 2007* (2007), p. 440.
- [41] N. DiMonte and C.-Y. Yao, in *Proceedings of ICALEPCS 2007* (2007), p. 550.
- [42] M. Hoffmann, S. Choroba, F. Eints, U. Hurdelbrink, P. Morozov, J. Randhahn, S. Ruzin, S. Simrock, E. Vogel, and R. Wagner, in *Proceedings of EPAC 2006* (2006), p. 2985.
- [43] J. Randhahn, S. Choroba, F. Eints, U. Hurdelbrink, M. Hoffmann, P. Morozov, Y. Nechaev, S. Ruzin, S. Simrock, and V. Soloviev, in *Proceedings of PAC 2007* (2007), p. 185.
- [44] Y. Kim, W. Wu, M. Busch, P. Wang, Y. K. Wu, D. Teytelman, I.-S. Park, and I. S. Ko, in *Proceedings of PAC 2007* (2007), p. 518.

- [45] M. Lonza, CERN Accelerator School: Digital Signal Processing p. 285 (2008).
- [46] S. Lee, *Accelerator Physics* (World Scientific, 1999).
- [47] A. Chao, P. L. Morton, and J. R. Rees, in *Proceedings of PAC 1979* (1979), p. 3343.
- [48] D. Teytelman, J. Fox, S. Prabhakar, J. Byrd, G. Stover, A. Drago, and M. Serio (2000).
- [49] T. Nakamura, in *Proc. 4th Ann. Meetings Particle Accelerator Soc. of Japan (in Japanese)* (2007), p. 121.
- [50] A. Drago, A. Gallo, A. Ghigo, M. Zobov, J. D. Fox, and D. Teytelman, *Phys. Rev. ST Accl. Beams* **6**, 052801 (2003).
- [51] Z. Zhou et al., to be presented at PAC 2009 (2009).
- [52] S. Khan, T. Knuth, A. Gallo, F. Marcellini, B. Sparato, and M. Zobov, in *Proceedings of PAC 1999* (1999), p. 1147.
- [53] M. Dehler, in *Proceedings of EPAC 2002* (2002), p. 2070.
- [54] M. Dehler, V. Schlott, D. Bulfone, M. Lonza, and R. Ursic, in *Proceedings of EPAC 2000* (2000), p. 1894.